Energy & Environmental Science

ROYAL SOCIETY OF CHEMISTRY

PAPER

View Article Online
View Journal | View Issue

Check for updates

Cite this: *Energy Environ. Sci.*, 2026, **19**, 2194

Looping-accelerated CO_2 mineralization for cost-competitive cementitious materials and hydrogen

Kyle Shank,[a] Hefei Xu,[a] Yunming Xu,[b] Amirmohammad Arjomand Kermani,[a] Jiangzhou Qin[a] and Shang Zhai *[ac]

Received 3rd December 2025,
Accepted 13th February 2026

DOI: 10.1039/d5ee07347b

rsc.li/ees

Advancing a net-negative carbon economy requires efficient and cost-effective CO_2 capture and utilization methods. Here, we introduce a novel sodium carbonate (Na_2CO_3) looping process that accelerates CO_2 capture and mineralization by silicate feedstocks such as steel slags, producing a carbonate-rich product and amorphous silica as cementitious materials. Unlike conventional direct or acid-assisted mineralization, our chemical looping approach first carbonates the silicate using a Na_2CO_3 solution. The resulting solution then reactively captures CO_2 and precipitates high-purity, (sub)micron-sized amorphous silica, while simultaneously regenerating Na_2CO_3. Demonstrated on steel slags, the process achieved 59% and 35% capture for point-source and air CO_2, respectively, mineralizing up to 2.79 mmol-C g^{-1} slag. Compared to traditional slag-water CO_2 mineralization, Na_2CO_3 looping captured and mineralized 4 to 9 times more CO_2. Mechanistically, Na_2CO_3 looping accelerates mineralization by rapidly removing Ca *via* carbonate precipitation, thereby sustaining a strong thermodynamic driving force for continued Ca–silicate dissolution, which governs the overall carbonation rate. The process offers several key advantages and novelties: (1) no net chemical consumption due to complete Na_2CO_3 regeneration; (2) CO_2 capture and mineralization occur at room temperature and 1 atm; (3) the CO_2 source can be either a point source or ambient air; (4) both the carbonation and reactive capture steps are exothermic, lowering system energy demand and eliminating external heat input; and (5) two cementitious products—carbonate-rich solids and amorphous silica—are generated separately, enabling flexible blending in downstream applications. Additionally, utilization of slag waste heat enables its reaction with steam to produce up to 1.01 mmol-H_2 g^{-1} slag. Without product revenues, levelized costs are only \$252 and \$50 per ton of CO_2 for air and point-source capture, respectively; considering product revenues, the payback periods are only 1.9 and 0.8 years for air and point-source CO_2.

Broader context

Achieving climate stabilization will require scalable technologies capable of permanently removing carbon dioxide (CO_2) from both industrial emissions and the atmosphere. Although direct air capture (DAC) is increasingly recognized as essential for addressing legacy and residual emissions, existing DAC approaches are often energy-intensive and producing concentrated CO_2 streams that require further handling and storage. Mineralization offers a fundamentally different pathway by converting CO_2 directly into stable solids, but most mineral carbonation routes remain limited by slow kinetics, high-temperature activation, or net chemical consumption. This study demonstrates a sodium carbonate looping process that couples CO_2 capture and accelerated mineralization in a fully regenerative cycle using steel slag, an abundant industrial waste. By regenerating the sodium carbonate under mild conditions and without chemical loss, the process enables permanent CO_2 storage while operating at substantially lower energy demand than conventional capture–storage systems. Importantly, the looping chemistry is compatible with both point-source CO_2 and atmospheric CO_2, providing a pathway for mineralization-enabled DAC. Beyond carbon removal, the process valorizes steel slag into supplementary cementitious materials, linking negative emissions with decarbonization of the cement and steel sectors. This integrated approach illustrates how chemical looping mineralization can support climate-relevant, circular solutions for large-scale carbon management.

Introduction

To reverse global warming, advancements to drive a net-negative carbon economy are essential;[1] current approaches to capture and store CO_2 from industrial flue gas and the

---

[a] *Department of Mechanical and Aerospace Engineering, The Ohio State University, 201 West 19th Ave, Columbus, OH, 43210, USA. E-mail: zhai.218@osu.edu*
[b] *Department of Chemical and Biomolecular Engineering, The Ohio State University, 151 W. Woodruff Avenue, Columbus, OH, 43210, USA*
[c] *School of Earth Sciences, The Ohio State University, 125 South Oval Mall, Columbus, OH, 43210, USA*

atmosphere are relatively expensive and have significant energy requirements. Traditional CO_2 capture processes, such as amine capture[2] and calcium looping,[3] usually require significant amount of heat or work to regenerate capture media. Additionally, these processes produce pure CO_2 gas requiring further treatment for permanent storage.

One pathway for permanent CO_2 storage is mineralization, which utilizes alkaline minerals and wastes to convert CO_2 into stable carbonates (stable up to 500 °C).[4] Commonly used alkaline minerals for mineralization include wollastonite,[5] serpentine,[6] and olivine.[7] Additionally, industrial wastes such as mine tailings,[8] fly ash,[9] recycled concrete,[10] and steel slags[11]—the focus of this research—are also used.

Relevant literature has established iron and steel slags as promising, plentiful, and cost-effective feedstocks for CO_2 capture and mineralization.[12] While blast furnace slag (iron slag) is commercially used as a supplementary cementitious material (SCM) to partially replace Portland cement,[13] basic oxygen furnace (BOF) and electric arc furnace (EAF) slags (two types of steel slags, with 260 million tons disposed annually[14,15]) have almost no use in concrete due to their free CaO and MgO contents, which cause expansive reactions,[16] and because their low pozzolanic reactivity limits their ability to contribute to cement hydration.[17] However, CO_2 mineralization can carbonate CaO and MgO producing a carbonate-rich product and silica that can be used as SCMs.[18] A recently published high temperature process produces calcium silicates and MgO for reactive CO_2 capture,[19] which are already abundant in steel slags.

Mineralization of steel slags is a promising solution for the permanent storage of CO_2.[20] However, direct mineralization methods are limited by slow reaction kinetics. For example, direct gas–solid and direct aqueous mineralization[21,22] can occur at low temperature and pressure, but reaction rates are slow—often taking hours to days—due to kinetic limitations.[16] To accelerate the process, temperature and CO_2 partial pressure are usually increased but with an energy penalty.[23] Another pathway to enhance mineralization rates is the indirect aqueous process, which uses inorganic acids or bases to dissolve magnesium or calcium silicates in alkaline solids, releasing ions that react with CO_2.[24] Although effective, this approach incurs additional material and processing costs due to chemical consumption.

Our work aims to leverage the enhanced mineralization rates of the indirect aqueous process, while avoiding chemical consumption through chemical looping. We propose a novel sodium carbonate (Na_2CO_3) looping process, in which silicate minerals such as steel slags are first carbonated with aqueous Na_2CO_3 to form a carbonate-rich product. The basic solution is then regenerated by capturing CO_2, simultaneously producing high purity precipitated amorphous silica. Compared to traditional mineralization routes, this process stands out in that the employed Na_2CO_3 gets fully regenerated and thus no chemical is consumed. Additionally, the separately precipitated amorphous silica introduces a highly pozzolanic and reactive phase that overcomes the inherently low pozzolanic reactivity of BOF steel slag.

Previous studies have explored coupling CO_2 capture and mineralization through chemical looping, but most rely on amine solvents such as monoethanolamine (MEA) or sodium glycinate. For example, Liu *et al.* demonstrated CO_2 absorption in amines followed by mineralization with Ca- or Mg-based oxides,[25] while Li *et al.* coupled MEA capture with lime kiln dust carbonation.[26] Although effective under controlled conditions, these methods relied on pure or concentrated CO_2 streams, depend on costly solvents less available than common alkalis, and do not generate a separable silica product. In addition, amine degradation and solvent loss remain major barriers to scale.

A closer parallel is the work of Li *et al.*, who investigated CO_2 capture with KOH to form potassium carbonate that then carbonated cement mortar waste.[27] While following an alkali looping process, their approach required 10% CO_2 feeds, suffered from significant KOH losses during cycling, and did not yield purified silica. A related study by Wu *et al.* examined the carbonation of ladle furnace slag using sodium bicarbonate, but their work was limited to a single batch cycle under pure CO_2 and focused on alumina extraction rather than isolating amorphous silica – which plays a dominant role, relative to alumina, in forming the primary cement hydration products.[28]

In contrast, our Na_2CO_3 looping process avoids many of the limitations observed in prior carbonation systems reported in the literature. In addition to beginning with Na_2CO_3, a weak, inexpensive, and widely available base, the process introduces several key advantages: it consumes no net chemicals due to full Na_2CO_3 regeneration; operates at room temperature and 1 atm; accommodates CO_2 from either point sources or air; and is driven by exothermic carbonation and capture steps that minimize external energy demand. It also produces two separate cementitious products—carbonate-rich solids and amorphous silica—enabling flexible blending in downstream applications.

Within the broader carbon capture, utilization, and storage (CCUS) landscape, mineralization-based utilization pathways differ from capture-and-storage approaches in that CO_2 is converted directly into stable solid products, avoiding the need for compression, transport, and geological storage. For alkaline solids, however, prior mineral carbonation strategies have generally required high-temperature silicate activation[29] or net chemical consumption[24] to achieve practical reaction rates. These tradeoffs motivate the development of chemical looping mineralization pathways that combine permanent CO_2 storage with accelerated kinetics under mild conditions and low energy and material inputs.

In addition to their CO_2 mineralization capacity, steel slags contain reduced iron species at +2 oxidation state that can be used for thermochemical hydrogen (H_2) production. H_2 can be produced from an exothermic reaction between steam and solid steel slag at 250–1000 °C[30] or molten steel slag at 1500–1600 °C.[31,32] The BOF process occurs at 1650 °C, thus the BOF slag temperature is sufficient for the thermochemical H_2 production.[33] Optionally, steel slag may be reacted with steam prior to mineralization to generate H_2, creating an additional pathway for integration with clean energy systems.

In this study, we implement a fully closed Na_2CO_3 looping cycle on steel slag and demonstrate stable, multi-cycle operation with significantly accelerated CO_2 mineralization under both point-source and air conditions, relative to conventional direct aqueous mineralization, and under mild operating conditions (24–45 °C, 1 atm). We quantitatively compare looping-based mineralization to direct aqueous carbonation and couple these experimental results with a technoeconomic analysis evaluating the co-production of SCMs and H_2, demonstrating progress toward a cost target of \$100 per ton-CO_2 captured from air.[34] Finally, we perform a mechanistic investigation to distinguish the reaction pathways unique to Na_2CO_3 looping from those governing direct aqueous mineralization.

Process description

The process includes steam to H_2 conversion and Na_2CO_3 looping for CO_2 mineralization (Fig. 1). Here, "mineralization" refers to CO_2 converted into stable carbonate phases (*e.g.*, $CaCO_3$) that remain locked below 500 °C, while "capture" also includes less stable forms such as bicarbonate.

BOF slag contains mainly calcium silicates, calcium oxide, calcium iron(III) oxide, and magnesium iron(II) oxide. Four different BOF slags were obtained from Cleveland-Cliffs – Cleveland Works: quenched, aggregate non-metallic, fines, and aged fines. Slag descriptions are provided in the Methods section and Fig. S1. The quenched BOF slag elemental composition was experimentally determined through inductively coupled plasma optical emission spectroscopy (ICP-OES) (Table S1).

In Step 1 (H_2 production), water vapor exothermically reacts with Fe^{2+} in steel slag to produce H_2 (eqn (1)). Additionally, the steam can make the slag brittle, so that milling becomes less energy intensive.[35] The H_2 production reaction is optional for Na_2CO_3 looping afterwards. The H_2 production results (Fig. S2 and S3) and discussion are available in the SI.

$$3FeO(s) + H_2O(g) \rightarrow Fe_3O_4(s) + H_2(g) \quad \Delta H(600\ ^\circ C) = -55.72\ kJ\ mol^{-1} \tag{1}$$

Step 2 (carbonation) is a set of exothermic reactions that carbonate the slag components, calcium silicates and calcium oxide, by Na_2CO_3 solution at 20–70 °C and 1 atm, producing sodium silicate (Na_2SiO_3) and sodium hydroxide (NaOH) solution and $CaCO_3$ precipitate to permanently store CO_2 (eqn (2)–(4)). The Na_2SiO_3 and NaOH solution is then filtered from the $CaCO_3$ and unreactive slag components (a mixture described as carbonate-rich product).

$$3Na_2CO_3(aq) + Ca_3SiO_5(s) + 2H_2O(l) \rightarrow Na_2SiO_3(aq) + 3CaCO_3(s) + 4NaOH(aq) \quad \Delta H(70\ ^\circ C) = -189.15\ kJ\ mol^{-1} \tag{2}$$

$$2Na_2CO_3(aq) + Ca_2SiO_4(s) + H_2O(l) \rightarrow Na_2SiO_3(aq) + 2CaCO_3(s) + 2NaOH(aq) \quad \Delta H(70\ ^\circ C) = -139.78\ kJ\ mol^{-1} \tag{3}$$

$$Na_2CO_3(aq) + CaO(s) + H_2O(l) \rightarrow CaCO_3(s) + 2NaOH(aq) \quad \Delta H(70\ ^\circ C) = -5.25\ kJ\ mol^{-1} \tag{4}$$

Step 3 (CO_2 capture) is a set of exothermic reactions (eqn (5) and (6)) that use the alkaline Na_2SiO_3 and NaOH solution from

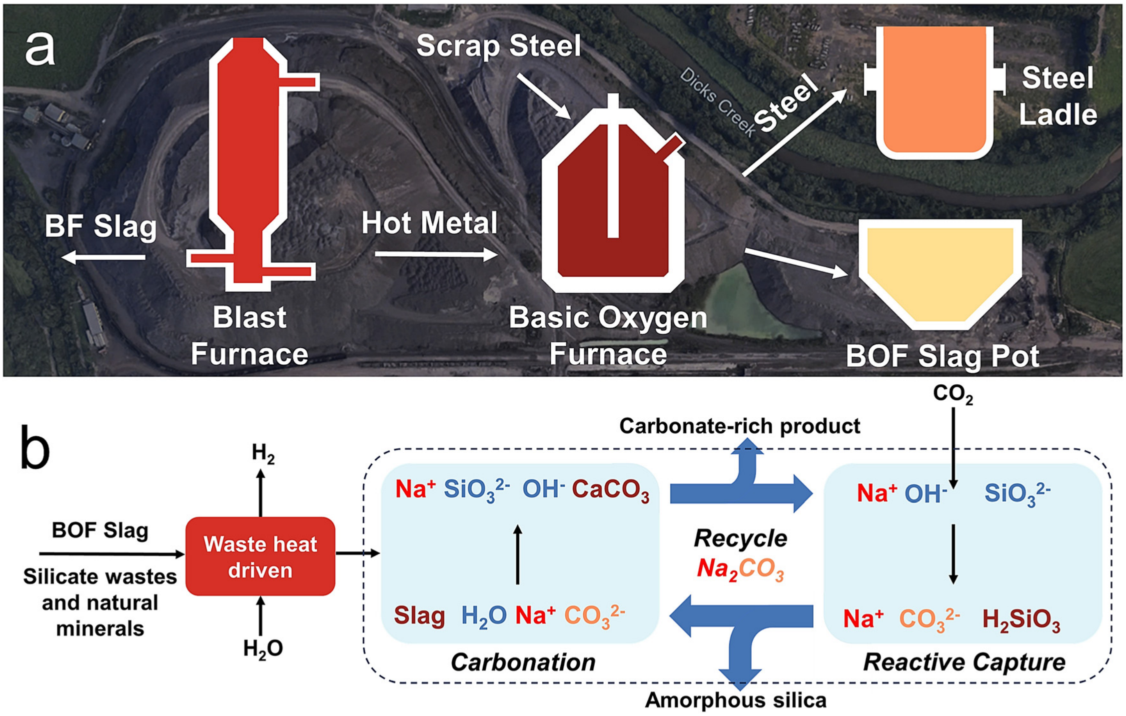

Fig. 1 (a) Basic oxygen furnace (BOF) steel slag generation process. (b) Hydrogen (H_2) production and sodium carbonate (Na_2CO_3) looping for CO_2 capture and mineralization by BOF steel slag or other silicate feedstock.

Step 2 to absorb CO_2 and form silicic acid (H_2SiO_3) precipitate; meanwhile, the Na_2CO_3 as well as part of H_2O consumed in Step 2 are regenerated.

$$2CO_2(g) + 2Na_2SiO_3(aq) + 2H_2O(l) \rightarrow 2H_2SiO_3(s) + 2Na_2CO_3(aq) \quad \Delta H(70\ ^{\circ}C) = -159.47\ kJ\ mol^{-1} \tag{5}$$

$$4CO_2(g) + 8NaOH(aq) \rightarrow 4H_2O(l) + 4Na_2CO_3(aq) \quad \Delta H(70\ ^{\circ}C) = -431.17\ kJ\ mol^{-1} \tag{6}$$

The H_2SiO_3 precipitate is then filtered for Step 4 to decompose it into silica (SiO_2) and water vapor (eqn (7)). This regenerates the remaining water consumed in Step 2. $< \sim 100\ ^{\circ}C$ heat is sufficient for the decomposition and can be supplied through the waste heat of slag. The decomposition is not required for Na_2CO_3 looping, but it generates valuable amorphous silica.

$$2H_2SiO_3(s) \rightarrow 2SiO_2(s) + 2H_2O(g) \quad \Delta H(100\ ^{\circ}C) = 72.87\ kJ\ mol^{-1} \tag{7}$$

Now, additional steel slag can be added, and the cycle can continue. Eqn (8) presents the overall Na_2CO_3 looping reaction (excluding H_2 production), which converts silicate feedstock and CO_2 into a stable carbonate and amorphous silica.

$$xCa_3SiO_5(s) + yCa_2SiO_4(s) + zCaO(s) + (3x + 2y + z)CO_2(g) \rightarrow (x + y)SiO_2(s) + (3x + 2y + z)CaCO_3(s) \tag{8}$$

Results and discussion

Na_2CO_3 looping performance

To evaluate Na_2CO_3 looping on steel slag mineralization (Step 2 and Step 3), we compared the Na_2CO_3 looping case to a direct aqueous baseline for both point-source and air CO_2 scenarios. These are referred to as "looping" and "baseline" in the following sections.

Point-source CO_2. The looping experiment consisted of four cycles, each including a carbonation (Step 2) and a CO_2 capture step (Step 3). In the looping case, 1 g of post-hydrogen-production quenched slag was reacted in an aqueous solution with a Na_2CO_3-to-slag mass ratio of 2.5 : 1 and a water-to-slag ratio of 50 : 1. The carbonation was carried out at 45 °C with a stirring rate of 400 rpm for 30 min.

After carbonation, the mixture was centrifuged to separate the carbonate-rich product from the solution. The solution was then used in the CO_2 capture step, where a 4% CO_2/Ar gas was flowed through the solution at 90 standard cubic centimeters per minute (sccm) for 30 min, followed by an Ar flush to help the exhaust gas analysis quantify the remaining CO_2 in the reactor. The capture duration was optimized to regenerate the Na_2CO_3 consumed during carbonation without further converting it into $NaHCO_3$. After each capture step, 1 g of fresh slag was added to the regenerated solution, and the cycle was repeated for a total of four times. Detailed experimental steps are provided in the methods sections.

The baseline experiment followed the same procedure but without Na_2CO_3 addition. In this case, the aqueous reaction served as a hydration step, releasing $Ca(OH)_2$ into solution, which then reacted with CO_2 during the capture step to form $CaCO_3$. The looping and baseline cases are visualized in Fig. S4a.

The 4% CO_2 concentration was selected to represent post-combustion flue gas from a natural-gas combined cycle power plant.[36] Other major flue gas components, such as N_2 and O_2, do not participate in reactions in the looping process under the conditions studied and primarily act as diluents; their effects are therefore expected to be equivalent to those of Ar in this system. Additionally, minor flue-gas contaminants (SO_x and NO_x) are typically reduced to low-ppm levels by upstream gas-conditioning processes and are therefore not expected to influence the chemistry studied here, as discussed further in the energy and technoeconomic analyses section.[37]

The cyclic performance of the looping and baseline cases is shown in Fig. 2a, along with a blank run (water only) representing the inlet CO_2. After four cycles, the CO_2 capture ratio of the looping system reached 59%, compared to only 7% for the baseline.

Thermogravimetric analysis (TGA) was conducted on the carbonate-rich product after the fourth looping cycle (Fig. S5a). The amount of mineralized CO_2 determined from TGA (3.17 mmol-C g^{-1} slag) was consistent with the CO_2 captured from the gas analysis (2.79 mmol-C g^{-1} slag), within a reasonable 15% deviation.

For the baseline, TGA indicated 0.29 mmol C g^{-1} slag (Fig. S5b), closely matching the 0.34 mmol-C g^{-1} slag measured from the gas capture side. These values are expected to be equivalent since $CaCO_3$ is the sole carbonation product formed during the capture step.

The pH and temperature measured after each step for the looping and baseline cases are shown in Fig. 2b. Taken together, the carbon balance and cyclic pH behavior provide strong evidence for closed-loop regeneration of Na_2CO_3 under the conditions studied. The carbon balance shown above demonstrates that the amount of CO_2 captured equals the amount carbonated in the fourth cycle, confirming mass closure across the looping sequence. In parallel, the stable cyclic pH observed in the looping system demonstrates that NaOH and Na_2SiO_3 formed during carbonation are fully consumed during CO_2 capture, returning the solution to its initial state each cycle and preventing accumulation of unused capture capacity. As shown in Fig. 2b, both the maximum pH after carbonation and the minimum pH after CO_2 capture return to essentially the same values on every cycle. If sodium or alkalinity were being lost from solution through irreversible $NaHCO_3$ formation or incorporation of Na into solid phases, the post-carbonation pH would be expected to decrease over successive cycles. Conversely, accumulation of unused alkaline capacity would lead to an upward drift in the post-capture pH. The absence of either trend indicates that the alkalinity generated during slag carbonation is fully consumed during CO_2 capture and subsequently regenerated in the following cycle.

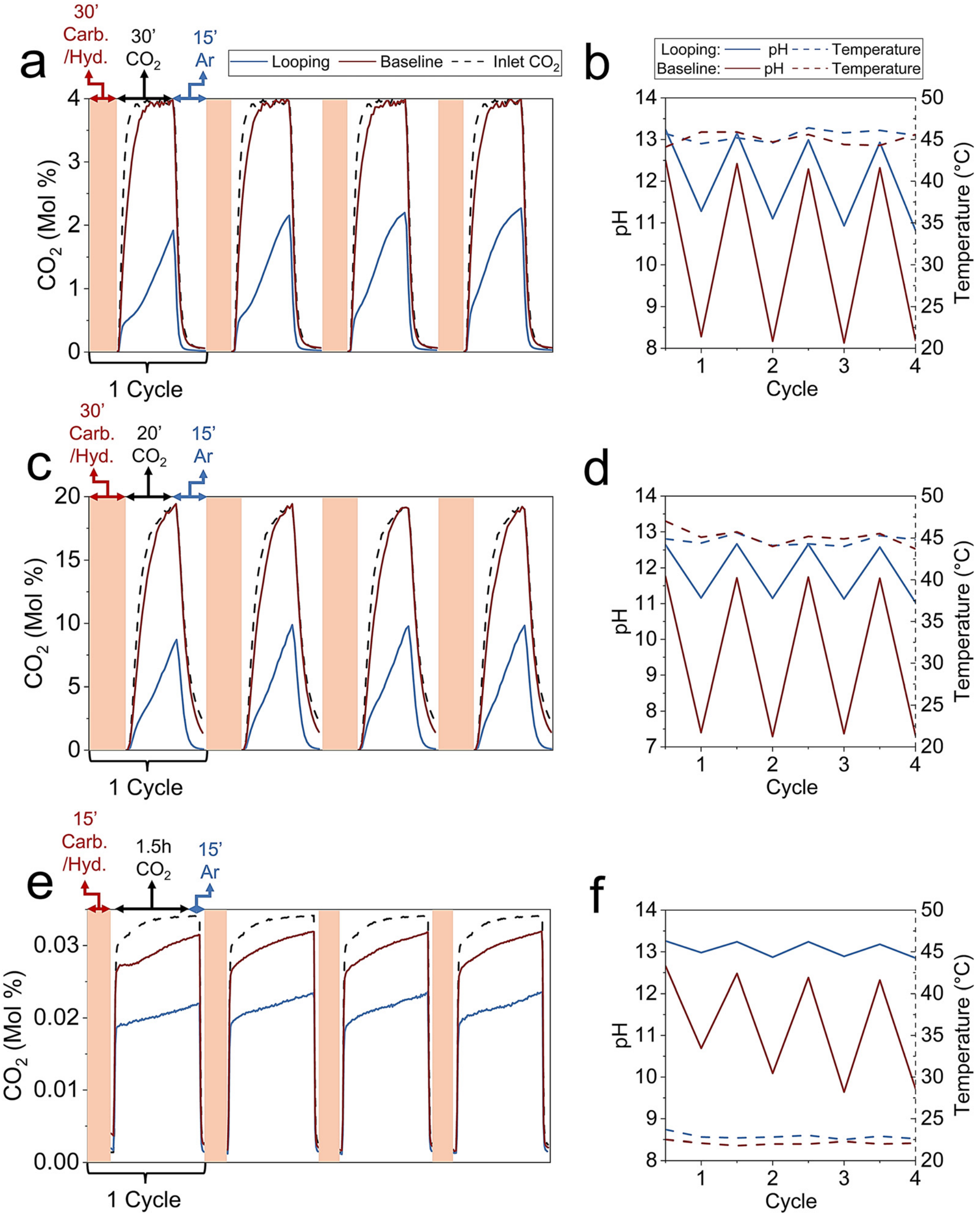

Fig. 2 (a) Four Na_2CO_3 looping cycles of 4% CO_2 with quenched BOF slag compared to the baseline; the conditions were 1 g slag per cycle, 45 °C, and 90 sccm 4% CO_2/Ar. (b) pH and temperature after each step in 4% CO_2 looping and baseline. Half cycles are after carbonation and full cycles are after CO_2 capture. (c) Four Na_2CO_3 looping cycles of 20% CO_2 with aged fines BOF slag compared to the baseline; the conditions were 10 g slag per cycle, 45 °C, and 90 sccm 20% CO_2/Ar. (d) pH and temperature after each step in 20% CO_2 looping and baseline. (e) Four Na_2CO_3 looping cycles of air CO_2 with quenched BOF slag compared to the baseline; the conditions were 0.05 g slag per cycle, 24 °C, and 90 sccm 343 ppm CO_2. (f) pH and temperature after each step in air CO_2 looping and baseline.

In addition, the solution pH remains above ∼11 throughout the looping experiments, a regime in which carbonate speciation is dominated by CO_3^{2-} rather than HCO_3^-. Under these conditions, any transient bicarbonate formed during CO_2 absorption is reconverted to carbonate during carbonation and does not accumulate.

The addition of Na_2CO_3 significantly enhanced both the CO_2 capture ratio and the extent of mineralization. Specifically, the looping system showed approximately nine times greater CO_2 capture ratio and CO_2 mineralization compared to the baseline. These results demonstrate the accelerated reaction kinetics and improved carbonation extent achieved through Na_2CO_3 looping.

Building on the 4% CO_2 experiments, a scaled-up test was conducted using 10 g of aged fines per cycle, a water-to-slag ratio of 20 : 1, and a 20% CO_2 gas stream to evaluate looping performance at higher dosages. Aged fines were selected because they represent an accumulation of slag from multiple production batches and have undergone environmental weathering, resulting in greater compositional variability. The 20% CO_2 was chosen to approximate the concentration of CO_2 in the flue gas of the BOF steel plant at Cleveland-Cliffs.

The cyclic performance of the 20% CO_2 looping and baseline is shown in Fig. 2c. After four cycles, the looping system achieved a CO_2 capture ratio of 69%, corresponding to 1.00 mmol-C g^{-1} slag, whereas the baseline case reached only 11% capture (0.15 mmol-C g^{-1} slag). Measurements of solution pH and temperature after each process step are shown in Fig. 2d.

Despite the increased slag mass, and the compositional variability of aged fines, the looping experiments retain the same kinetic advantage observed in the 1 g quenched slag tests. This result confirms that the Na_2CO_3 looping mechanism remains effective at higher dosages and for more heterogeneous slag feedstocks.

Air CO_2. For these experiments, the same Na_2CO_3 looping procedure was applied with adjusted reaction conditions. In the looping case, 0.05 g of post-hydrogen-production quenched slag was reacted in an aqueous solution with a Na_2CO_3-to-slag ratio of 1 : 1 and a water-to-slag ratio of 100 : 1. The carbonation step was conducted at room temperature (24 °C) with a stirring rate of 400 rpm for 15 min.

Following carbonation and separation, the solution was exposed to 343 ppm CO_2 (from a compressed air cylinder) at 90 sccm for 1.5 h, followed by an Ar flush. After each capture step, 0.05 g of fresh slag was added to the regenerated solution, and the cycle was repeated four times. A corresponding baseline experiment without Na_2CO_3 addition was performed for comparison.

The cyclic performance of the air CO_2 looping and baseline cases is shown in Fig. 2e. After four cycles, the looping system achieved 35% CO_2 capture, compared to 9% for the baseline. The pH and temperature for the processes are shown in Fig. 2f, demonstrating cyclic behavior under looping conditions similar to the point-source cases.

TGA of the carbonate-rich product after the fourth looping cycle (Fig. S5c) indicated 0.93 mmol-C g^{-1} slag mineralized, consistent with 0.83 mmol-C g^{-1} slag measured from gas analysis. For the baseline, insufficient $CaCO_3$ was recovered for TGA due to the small slag amount, but 0.23 mmol-C g^{-1} slag was quantified from the gas capture data.

The Na_2CO_3 looping system demonstrated a substantial enhancement in air CO_2 performance, achieving a four times higher CO_2 capture ratio and CO_2 mineralization than the baseline. Although the overall capture efficiency was lower than in the point-source case (as expected due to the dilute CO_2 concentration), the looping process maintained stable regeneration and carbonation across cycles, confirming its feasibility for continuous operation with air CO_2.

Silica production. Because only small quantities of slag were processed during the looping experiments, the amount of precipitated silica was insufficient to isolate after each cycle. Therefore, a single large-scale carbonation experiment with an extended CO_2 capture step under pure CO_2 was conducted to generate enough material for characterization (details in Fig. S6). The resulting high purity amorphous silica was confirmed by X-ray diffraction (XRD) and scanning electron microscopy (SEM) coupled with energy-dispersive X-ray spectroscopy (EDS), as shown in Fig. S6. SEM images also revealed (sub)-micron-sized silica particles. Complementary ICP-OES analysis (Table S2) further indicated minimal contamination from other elements.

Energy and technoeconomic analyses

Energy and technoeconomic analyses were conducted for H_2 production and CO_2 mineralization. Four scenarios were analyzed: point-source capture and mineralization by Na_2CO_3 looping and baseline as well as air CO_2 by Na_2CO_3 looping and baseline. The Na_2CO_3 looping scenarios followed the reactions detailed in the Process description section. In contrast, the baseline scenarios employed modified Steps 2 and 3 to first hydrate the slag, thereby releasing $Ca(OH)_2$ into solution, which subsequently reacted with CO_2 to form $CaCO_3$. Detailed technoeconomic analysis methods are available in the SI.

The analysis is based on our experimental results using quenched slag as described in the Na_2CO_3 Looping Performance section. CO_2 mineralization capacities were 2.79, 0.32, 0.83, and 0.23 mmol-C g^{-1} slag for point-source looping, point-source baseline, air CO_2 looping, and air CO_2 baseline, respectively. FeO content was estimated from experimental H_2 production (0.76 mmol-H_2 g^{-1} slag). TGA data was combined with XRD refinement (Table S3) to determine the mols of actively reacted components, namely calcium silicates and CaO (Table S4). Annually 100 000 tons of CO_2 captured and mineralized are used for the mass balance in each scenario (Table S5).

Reaction temperatures were optimized to reduce external cooling and heating. All reactions were exothermic except silicic acid decomposition, which was driven by waste heat from slag. Secondary processes require electricity for conveying, milling, filtering, stirring, pumping, and fan-driven gas flow. Four electricity sources were evaluated for each scenario: (1) external solar grid, (2) internal solar photovoltaic (PV) system with integrated 16-hour battery storage, (3) internal wind turbines with integrated 16-hour battery storage, and (4) internal steam power plant using slag waste heat (Table S6).

The capital cost of the system was estimated using engineering design books.[38,39] The gas/air contactor system was designed based on Carbon Engineering's air-contactor configuration, incorporating a slab contactor with packing for efficient gas–liquid contact, as well as fans for gas/air movement and pumps for circulating the absorption solution.[40] The plant was assumed to have a lifetime of 50 years, and the lifespan of the equipment was estimated to determine a replacement schedule (Table S7).

Point-source CO_2. Fig. 3a presents the preliminary plant design for point-source Na_2CO_3 looping, while Fig. 3b compares the process costs and revenue per ton-CO_2 to the baseline with a plant design shown in Fig. S7a. Cost components are detailed in Table S8. Na_2CO_3 looping is more cost-effective than

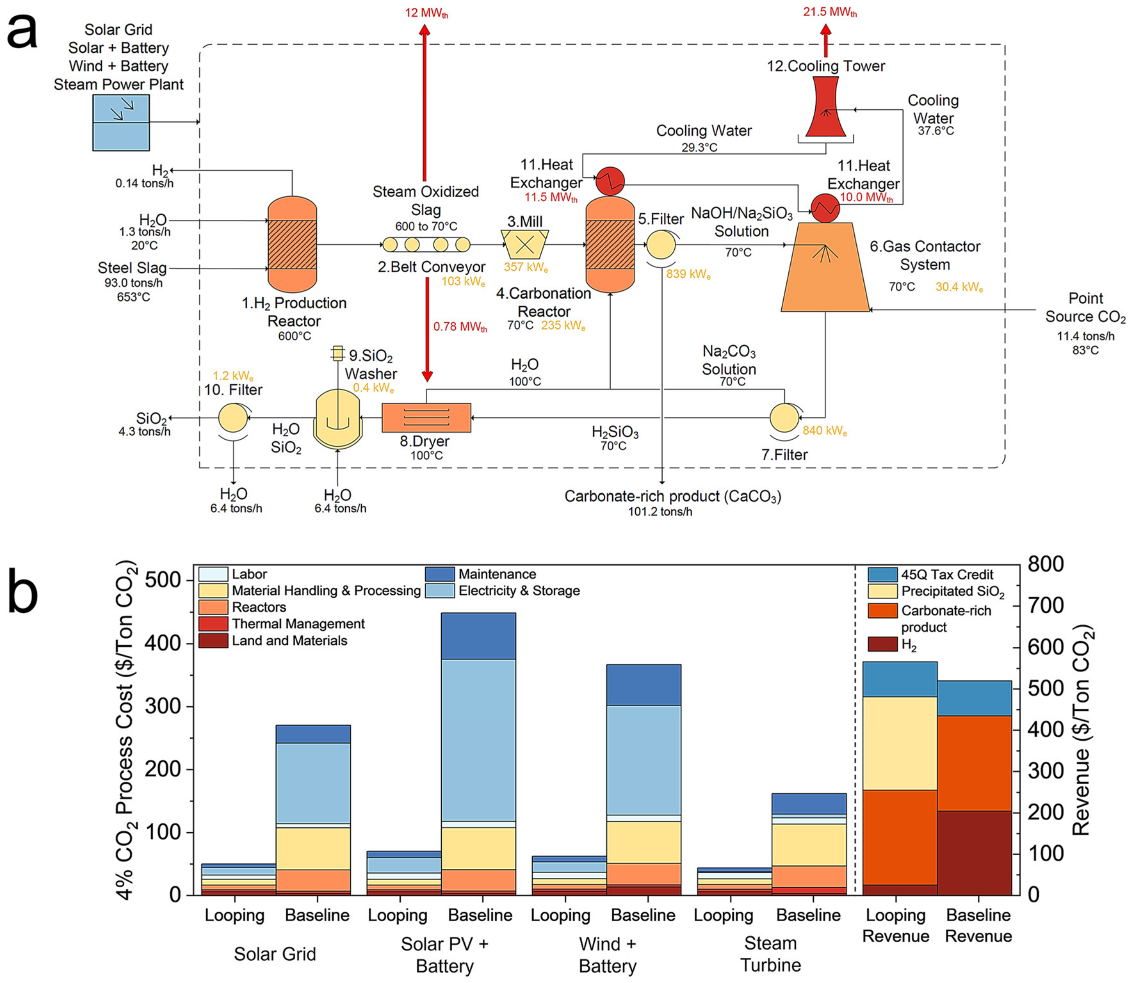

Fig. 3 (a) Proposed plant design for hydrogen (H_2) production and point-source CO_2 mineralization through Na_2CO_3 looping using BOF steel slag. (b) Technoeconomic analysis (TEA) comparing Na_2CO_3 looping to the baseline process for 4% CO_2. The process cost was evaluated for different energy (purely electricity) supply methods, including solar grid, internal solar PV with 16-hour battery storage, internal wind turbine with 16-hour battery storage, and an internal steam power plant using waste heat from the slag. The levelized costs of electricity are noted in Table S17. The revenue streams from 45Q tax credit, precipitated silica (SiO_2), carbonate-rich product, and H_2 are presented on the right axis.

the baseline, primarily due to reduced slag usage, enabling smaller reactors and lower electricity consumption. Installed equipment costs are provided in Tables S9–S12 for both scenarios, and Fig. S8 shows capital and operating cost breakdowns for Na_2CO_3 looping, with the major contributors being the carbonation reactor, vacuum filters for solid–liquid separation, the mill for slag crushing, the cooling tower and heat exchanger for thermal management, and electricity. Depending on the electricity source, process costs range from \$44 to \$70 per ton-CO_2 (excluding revenues) for the Na_2CO_3 looping system, while energy demands are 211 and 2215 kWh_e per ton-CO_2 for Na_2CO_3 looping and baseline, respectively.

The analysis incorporates revenue from several sources: H_2 sold at \$2 per kg,[41] precipitated silica at \$600 per ton,[42] and the 45Q tax credit providing \$85 per ton-CO_2 for CO_2 conversion into useful products.[43] The precipitated silica is assumed to be comparable to silica fume, an amorphous silica byproduct widely used as a SCM, for which reported market prices typically range from approximately \$150–800 per ton; the assumed value of \$600 per ton therefore represents a mid-range benchmark for a high-purity SCM product.[44] The selling price of the point-source Na_2CO_3 looping carbonate-rich product was assumed to be \$26 per ton.[45] This value was intentionally selected to be conservative relative to established SCMs such as ground granulated blast furnace slag (GGBFS), which typically sells for approximately \$36–38 per ton due to its well-established performance and market acceptance.[46] The baseline carbonate-rich product was assumed to be a mixture of the precipitated $CaCO_3$ and hydrated steel slag outputs to be comparable to the looping case. The selling price of the baseline carbonate-rich product was proportionally scaled to have equal yearly revenue for the carbonate-rich product in the looping case, considering the larger amount and lower quality (due to the lower carbonation extent) of the product in the baseline case compared to looping. With these revenue streams, the point-source Na_2CO_3 looping achieves a breakeven time of 0.8 years.

Air CO_2. Fig. 4a shows the preliminary plant design for Na_2CO_3 looping for air CO_2, while Fig. 4b compares the process costs and

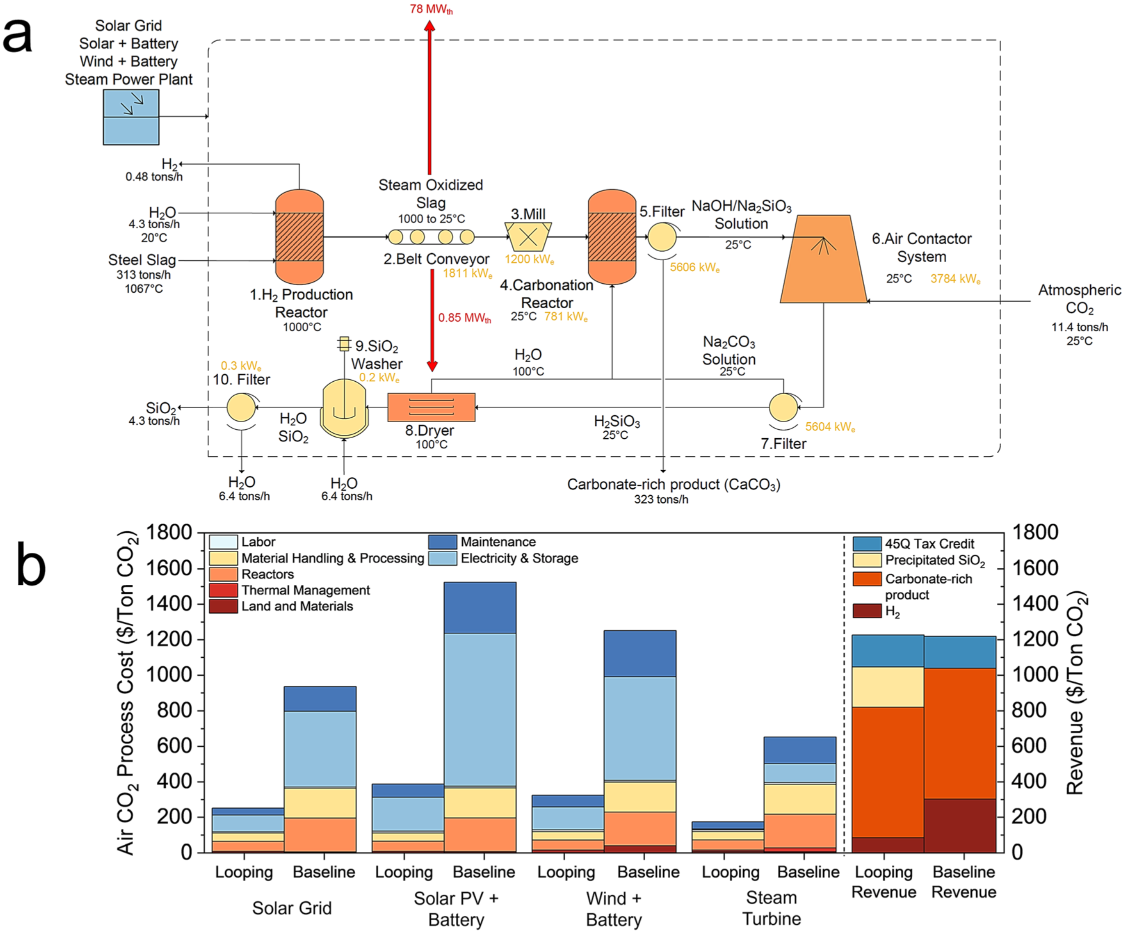

Fig. 4 (a) Proposed plant design for hydrogen (H_2) production and air CO_2 mineralization through Na_2CO_3 looping with BOF steel slag. (b) Technoeconomic analysis (TEA) comparing Na_2CO_3 looping to the baseline process for 343 ppm CO_2. The process cost was evaluated for different energy (purely electricity) supply methods, including solar grid, internal solar PV with 16-hour battery storage, internal wind turbine with 16-hour battery storage, and an internal steam power plant using waste heat from the slag. The levelized costs of electricity are noted in Table S17. The revenue streams from H_2, precipitated silica (SiO_2), carbonate-rich product, and the 45Q tax credit are presented on the right axis.

revenue per ton-CO_2 to the baseline with a plant design shown in Fig. S7b. The looping scenario outperforms the baseline. For the air CO_2 system there is no need for the heat exchanger and cooling tower in the solar grid, solar PV with battery, or wind turbine with battery scenarios, as the 25 °C air flow removes reaction heat.

However, the steam power plant still requires it for the condenser. The process equipment costs are detailed in Tables S13–S16, and Fig. S9 shows capital and operating cost breakdowns for Na_2CO_3 looping. The major cost contributors for air CO_2 include the air contactor system, vacuum filters, mill, carbonation reactor, and electricity. The air CO_2 Na_2CO_3 looping process costs between \$175 to \$388 per ton-CO_2 (excluding revenues), aiming towards the Department of Energy's \$100 per ton of air CO_2 goal by 2032.[34] Energy demand is 1646 kWh_e per ton-CO_2 for Na_2CO_3 looping and 7412 kWh_e per ton-CO_2 for the baseline. Including revenue, the breakeven time for air CO_2 Na_2CO_3 looping is 1.9 years, with a 45Q tax credit providing \$180 per ton-CO_2 for converting CO_2 from air into useful products.[43] The assumed levelized cost of electricity (LCOE) for each scenario is reported in Table S17.

The technoeconomic analysis presented here is informed by gram-scale experiments and is intended to assess the system-level feasibility and relative performance of Na_2CO_3 looping compared to baseline mineralization pathways. While kilogram-scale or larger systems are ultimately required to fully capture reactor-level heat and mass transfer, solids handling, and feedstock conditioning effects, these considerations do not alter the underlying material and energy balances evaluated here. Rather, they motivate subsequent larger-scale studies focused on energy requirements, slag type variability, and thermal management.

Implications for scale-up. Although the looping reactions are exothermic, the overall process requires 211–1646 kWh_e per ton-CO_2 for secondary unit operations, making electricity a major operating cost driver. To clarify the origin of this demand, the electrical energy contributions from individual unit operations are broken down in Fig. S10. These results show that solid–liquid separation is a dominant contributor to both capital and operating expenses (Fig. S8–S10).

It is important to note that the vacuum filtration costs include both the filtration equipment and the associated vacuum pumps, and the reported electrical demand reflects the combined power requirements of these components. Similarly, the gas–liquid contactor capital and operating expenses include both fans for gas flow and pumping for solution circulation. In the laboratory-scale experiments, centrifugation was used to minimize material losses; however, the scale-up analysis assumes vacuum filtration rather than centrifuges, reflecting substantially lower capital and operating costs at industrial scale.

At scale, filtration throughput directly determines equipment sizing and power consumption, making it a key engineering design variable. Fouling and filter-cake buildup are anticipated risks and will depend strongly on particle size distribution and slurry viscosity. Effective management of cake formation and fouling will be essential to avoid downtime associated with filter cleaning or replacement.

Because filtration costs scale with solution volume, the water-to-slag ratio is a key variable for cost optimization. The high ratios used in our laboratory experiments (20–100 : 1) were selected for small-scale validation; future optimization at scale to hopefully reduce liquid volume would directly affect pumping requirements, filtration duty, and equipment sizing. As an alternative, gravity clarification basins could partially or fully replace mechanical filtration, significantly lowering electrical power demand at the expense of a larger plant footprint. These tradeoffs highlight solid–liquid separation as a critical focus area for future process optimization and pilot-scale development.

Even with water recycling, industrial systems must manage hydraulic circulation, evaporation losses, and pumping energy. In the present analysis, water input is considered for the H_2 production step in both the baseline and Na_2CO_3 looping cases. In the baseline process, additional makeup water is required to account for water retained in hydrated calcium silicate phases. In contrast, the Na_2CO_3 looping case does not require makeup water for hydration or carbonation; water is fully conserved within the internal looping process, with a separate, steady water throughput associated with the silica washing step. Although water is temporarily consumed during slag carbonation, it is released during subsequent CO_2 capture and silicic acid drying steps, resulting in no net depletion of process water.

Evaporation losses within the process are expected to be modest, and the resulting makeup water requirement contributes negligibly to operating cost, consistent with assumptions made in prior analyses of aqueous CO_2 capture systems.[40] Pumping power and pressure drop are explicitly included in the present analysis across four stages: post-carbonation filtration, gas–liquid contactor circulation, post-contactor filtration, and silica washing and filtration.

Feedstock heterogeneity and process control are also critical considerations for scale-up. BOF slags are inherently heterogeneous, with batch-to-batch variations in free CaO content and calcium silicate phase distributions that can influence CO_2 mineralization capacity. As evaluated in the four-slag comparison presented later in this study (Mechanism study section), these compositional differences result in only minor variations in mineralization performance at the laboratory scale. At the industrial scale, greater feedstock variability is expected; however, product consistency can be maintained through appropriate process monitoring and control.

Because the Na_2CO_3 looping process both generates and consumes alkalinity within each cycle, the primary control objective is the consistent return of the solution to the same pH at the end of each CO_2 capture–carbonation sequence. Achieving a consistent cyclic pH confirms that alkalinity generation during carbonation is balanced by alkalinity consumption during CO_2 capture, independent of moderate variations in slag composition. Continuous pH monitoring therefore provides a practical feedback control strategy to accommodate feedstock heterogeneity while maintaining stable looping performance and a reproducible carbonate-rich SCM product.

Flue gas composition variability is another important consideration for industrial deployment. The point-source CO_2 experiments in this study employed a 4% CO_2/Ar mixture rather than flue gas. In industrial practice, however, flue gas is typically conditioned upstream using established air-pollution control technologies that reduce SO_x and NO_x concentrations to the low-ppm range for natural-gas combustion sources.[37] At these levels, SO_x and NO_x are more than three orders of magnitude lower than CO_2 concentrations and are therefore not expected to significantly compete with carbonate chemistry in the alkaline Na_2CO_3/NaOH system. Additionally, the presence of N_2 and O_2 in the flue gas is not expected to participate in the looping chemistry.

Particulate matter is likewise removed upstream by standard particulate control equipment, resulting in low contamination to downstream capture systems. As a result, implementation of the Na_2CO_3 looping process downstream of conventional flue gas cleanup is expected to face minimal additional risk from flue gas impurities. Nevertheless, integration with upstream gas conditioning and validation under representative flue gas compositions will be important considerations for future pilot-scale demonstrations.

Sensitivity to the CO_2 capture ratio was also evaluated as part of the scale-up analysis. Process costs were assessed for a ±20% variation around the experimentally observed capture ratios for both the point-source and air cases using a solar-grid electricity scenario (Fig. S11). For the point-source case, varying capture efficiency from 59% to 47% or 71% results in changes in the cost per ton of CO_2 of only approximately ±0.3%. This weak dependence reflects the dominance of solids handling and filtration costs and the relatively small gas-handling requirements at elevated CO_2 concentration.

In contrast, the air case exhibits a stronger dependence on capture ratio due to the much larger gas-handling equipment required at low CO_2 concentration. Varying capture efficiency from 35% to 28% and 42% results in cost changes of +8.6% and −5.8%, respectively. Even in this case, the overall cost variation remains within approximately +9/−6% for a ±20% change in capture ratio, indicating that the technoeconomic conclusions are robust to realistic variations in capture performance.

The deployment scale of the Na_2CO_3 looping process will be constrained by slag availability and transportation. To minimize handling and transport of intermediates, the looping system is envisioned to be co-located with steel plants, where fresh BOF slag and CO_2 streams are readily accessible. This configuration eliminates the need to ship raw slag to a separate processing site and enables air or direct point-source capture from steelmaking exhaust. Shipment of the carbonate-rich product and amorphous silica products aligns with existing logistics, as GGBFS is routinely transported from steel mills to cement plants. Because cementitious materials are bulk commodities, their economic transport radius is generally regional, with analyses indicating that most cement is distributed and consumed within ∼200 miles of the production facility.[47]

Using slag generation data from a representative U.S. steel mill (Cleveland-Cliffs Burns Harbor; 4–5 million tons-steel per year)[48] and an estimated 126 kg BOF slag per ton of steel,[15] a large BOF plant produces ∼2000 tons of slag per day. In the point-source case, a 100 000 ton-CO_2 per year facility requires approximately 2230 tons slag per day, which is within the same order of magnitude as the slag output of a single BOF plant. In practice, looping capacity would be matched to local slag availability rather than fixed at a nominal capture rate; because the slag requirements are comparable, the per-ton CO_2 cost estimates remain valid for point-source deployment.

For the air case, the slag requirement for a 100 000 ton-CO_2 per year facility (∼7500 tons slag per day) exceeds the output of a single U.S. steel plant; however, this requirement is comparable to the upper end of slag production from large integrated steel facilities worldwide, which can produce up to ∼14 million tons of steel per year, corresponding to ∼5000 tons slag per day.[49] Accordingly, the air case is treated as a normalized benchmark scenario. In practice, deployment would likely involve smaller looping units scaled to individual plants, integration of legacy slag and multiple alkaline feedstocks (cement kiln dust, fly ash, mine tailings, *etc.*), or aggregation of slag from multiple steel mills within a region. Re-evaluating the air-case with solar grid at a slag BOF throughput consistent with the point-source case (∼30 000 ton-CO_2 per year) yields a cost of $271 per ton-$CO_2$, compared to $252 per ton-$CO_2$ for the 100 000 ton-CO_2 per year. This corresponds to an increase of only ∼7%, indicating that the economics remain favorable when scaled to realistic slag availability.

In addition to slag throughput, air capture imposes higher gas–liquid contacting requirements than point-source operation due to the dilute CO_2 concentration giving limited mass transport. As a result, achieving cyclic stability under air conditions requires either increased CO_2 supply by supplying more air and/or limiting the extent of slag carbonation per cycle, thereby reducing the amount of NaOH and Na_2SiO_3 that must be consumed during capture. From an economic perspective, it may be advantageous to accept lower per-cycle slag conversion while maintaining shorter cycle times and lower equipment capital cost, provided that overall throughput and material utilization remain favorable.

Silica precipitation behavior is another important consideration for scale-up and product quality. Under the strongly alkaline conditions maintained in the looping system ($pH \geq 11$), silica is observed to remain as a dispersed colloidal suspension rather than forming a bulk gel. This results in a free-flowing slurry that can be circulated through the gas–liquid contactor and filtered downstream without excessive buildup, consistent with prior reports showing increased silica solubility at high pH.[50] If maximizing silica recovery is desired, pH provides an effective control variable: controlled CO_2 addition can be used to lower pH and induce precipitation to a targeted extent while preserving flowability.

Regarding silica impurities, aluminum released during carbonation is expected to precipitate as amorphous aluminosilicate, which can beneficially participate in calcium aluminosilicate hydrate (C–A–S–H) formation during cement hydration. Iron incorporation is expected to be low and comparable to that reported for commercial silica fume (<1 wt%), where Fe-bearing phases act primarily as benign fillers rather than strength-limiting components.[52] Finally, silica particle size represents a tunable design parameter. Prior studies show that gas–liquid contactor conditions, such as superficial gas velocity, influence silica nucleation and growth, providing a pathway to tailor particle size distribution.[53] Because finer amorphous silica exhibits higher pozzolanic reactivity and greater market value in cementitious applications, particle size control represents an additional opportunity to optimize both performance and revenue at scale.[54]

Literature benchmarking

To contextualize the performance of the Na_2CO_3 looping process, a quantitative comparison with mineralization and looping-based systems from the literature is provided in Table 1. Relative to prior alkali-looping mineralization routes, the point-source Na_2CO_3 looping process demonstrated here achieves CO_2 capacities on steel slag that are comparable to those reported for other alkaline wastes, while operating at substantially shorter cycle times. Notably, the present process operates at the lowest CO_2 concentration (4% and air CO_2) and among the mildest temperatures reported for looping-based mineralization systems, while also demonstrating stable looping performance under air CO_2 conditions that have not been quantitatively evaluated in previous studies.

Unlike most prior research, which discusses energy requirements qualitatively, this study provides a quantified energy analysis for the complete looping process. While similar looping configurations may ultimately exhibit comparable energy demands, such analyses have not previously been reported. When compared to high-temperature silicate activation routes, which require substantial thermal input for mineral activation, the point-source Na_2CO_3 looping process operates at lower energy demand under mild conditions. In the air Na_2CO_3 looping case, operation with atmospheric CO_2 results in reduced CO_2 capacity and higher energy intensity on a per-ton-CO_2 basis; however, this tradeoff enables rapid cycling under ambient conditions and serves as a benchmark for demonstrating the feasibility of closed-loop mineralization directly from air.

Finally, the Na_2CO_3 looping process uniquely demonstrates closed-loop regeneration of the carbonate carrier without observable loss. This behavior is demonstrated in the Na_2CO_3 Looping Performance section and is supported by stable cyclic pH

Table 1 Benchmarking of CO_2 mineralization and looping-based systems

Route	Feedstock	CO_2 Capacity (g_{CO_2} kg_{solid}^{-1})	Kinetics	Operating conditions	Energy demand	Chemical consumption/loss
Monoethanolamine (MEA) (Liu *et al.* 2021)[25]	Pure CaO, $CaSiO_3$, MgO	CaO: 776 $CaSiO_3$: 136 MgO: 727	3 h batch carbonation and capture	75 °C; 1 atm CO_2	Thermal heating with pure CO_2; no quantified analysis	Regeneration of MEA demonstrated qualitatively; solvent losses not quantified
MEA looping (Li *et al.* 2024)[26]	Lime Kiln dust	236	4–7 h carbonation	60 °C; 10% CO_2	External heat could be supplied from exothermic reactions and hot flue gas; no quantified analysis	CO_2 absorption capacity recovery ~90% after four mineralization cycles; MEA mass recovery not quantified; solid washing required and post-wash MEA concentration remains challenging
KOH looping (Li *et al.* 2024)[27]	Mortar waste	112	7 h capture and carbonation	Ambient temperature; 10% CO_2	Ambient conditions; no quantified analysis	KOH loss to solid–liquid separation and dilution; CO_2 absorption capacity decreases ~47% after 10 cycles
$NaHCO_3$ looping (Wu *et al.* 2023)[28]	Ladle furnace slag	244	4 h capture and carbonation	25–60 °C; pure CO_2	Ambient conditions with pure CO_2; no quantified analysis	pH recovery shown from CO_2 flow; no mass balance or multi cycle stability
High-temperature silicate activation (Gerdemann *et al.* 2007)[51]	Serpentine, wollastonite, olivine	Olivine: 450 Wollastonite: 293 Serpentine: 438	≤2 h heat treatment; 1–12 h carbonation	630 °C heat treatment; 40–150 atm CO_2, 100–185 °C carbonation	429–2431 kWh per ton_{CO_2} (thermal and electric)	Buffered $NaHCO_3$ solution used as CO_2 carrier; no chemical looping or regeneration demonstrated
Thermochemical activation of Mg-rich silicates (Chen and Kanan 2025)[19]	Olivine, serpentine, augite (Mg-rich silicates) + $CaCO_3$ or $CaSO_4$ (CaO source)	$CaCO_3$ + Mg_2SiO_4 : 519	1–4 h thermochemical activation; 2–7-week carbonation under air or <2 h under 1 atm CO_2	1100–1200 °C thermochemical activation; ambient temperature carbonation with air or 1 atm CO_2	510–1300 kWh per ton_{CO_2} (thermal and electric)	Consumes $CaCO_3$ or $CaSO_4$ as CaO source; requires sequestration of process CO_2; no demonstrated Ca looping
Point-source Na_2CO_3 looping (this study)	BOF steel slag	123	1 h capture and carbonation	45 °C; 4% CO_2	211 kWh per ton_{CO_2} (electric)	Closed-loop Na_2CO_3 regeneration demonstrated *via* carbon mass balance and stable cyclic pH
Air Na_2CO_3 looping (this study)	BOF steel slag	37	1.75 h capture and carbonation	Ambient temperature; air	1646 kWh per ton_{CO_2} (electric)	

behavior and a carbon mass balance indicating equivalent CO_2 capture and subsequent carbonation within a single cycle, in contrast to the solvent dilution, degradation, or loss commonly reported for amine- and hydroxide-based systems.

Mechanism study

The previous Na_2CO_3 Looping performance section used experimental conditions designed to test more realistic process operation (relatively lower water-to-slag ratio and separation of slag and solution between cycles) and provide input data for the technoeconomic analysis. In this section, we adopt an alternative procedure to distinguish the mechanistic differences between Na_2CO_3 looping and direct aqueous carbonation. This approach decouples the effects of slag and Na_2CO_3 by physically separating them into two reactors connected in series, enabling isolation of individual reaction pathways and verification of whether a new mineralization mechanism emerges under looping conditions.

The mechanism study included four experimental cases: a Na_2CO_3 looping case, two control cases, and one blank run (Fig. S4b). In the Na_2CO_3 looping case, steel slag was first carbonated with a Na_2CO_3 solution (Step 2), after which CO_2 at certain concentration was flowed through the reactor (Step 3). The control cases used two separate mixtures: a slag–water mixture and a Na_2CO_3 solution. In these control cases, Step 2 involved hydration of the steel slag, followed by CO_2 capture in Step 3. In the first control, CO_2 was first exposed to the Na_2CO_3 solution, then to the slag–water mixture; in the second, this order was reversed. The blank run measures the supplied CO_2 concentration profile.

A major procedural difference from the Na_2CO_3 looping performance tests is that the slag and solution were not separated after each cycle in the mechanism study cycles.

Each cycle was conducted at 45 °C and lasted 80 minutes: 45 minutes for carbonation or hydration, 15 minutes of 4% or 343 ppm CO_2 flow, and a 20-minute pure Ar flow to flush the remaining CO_2 for gas quantification. The slag samples were first reacted with steam for H_2 production before Step 2 and 3, unless stated otherwise.

Point-source CO_2. For point-source capture, 0.5 g of steel slag was processed each cycle with 90 sccm of 4% CO_2/Ar. The CO_2 capture performance for quenched slag over 10 Na_2CO_3 looping cycles is depicted in Fig. 5a, compared to the controls and blank run. The 10 cycles showed stability with an average of

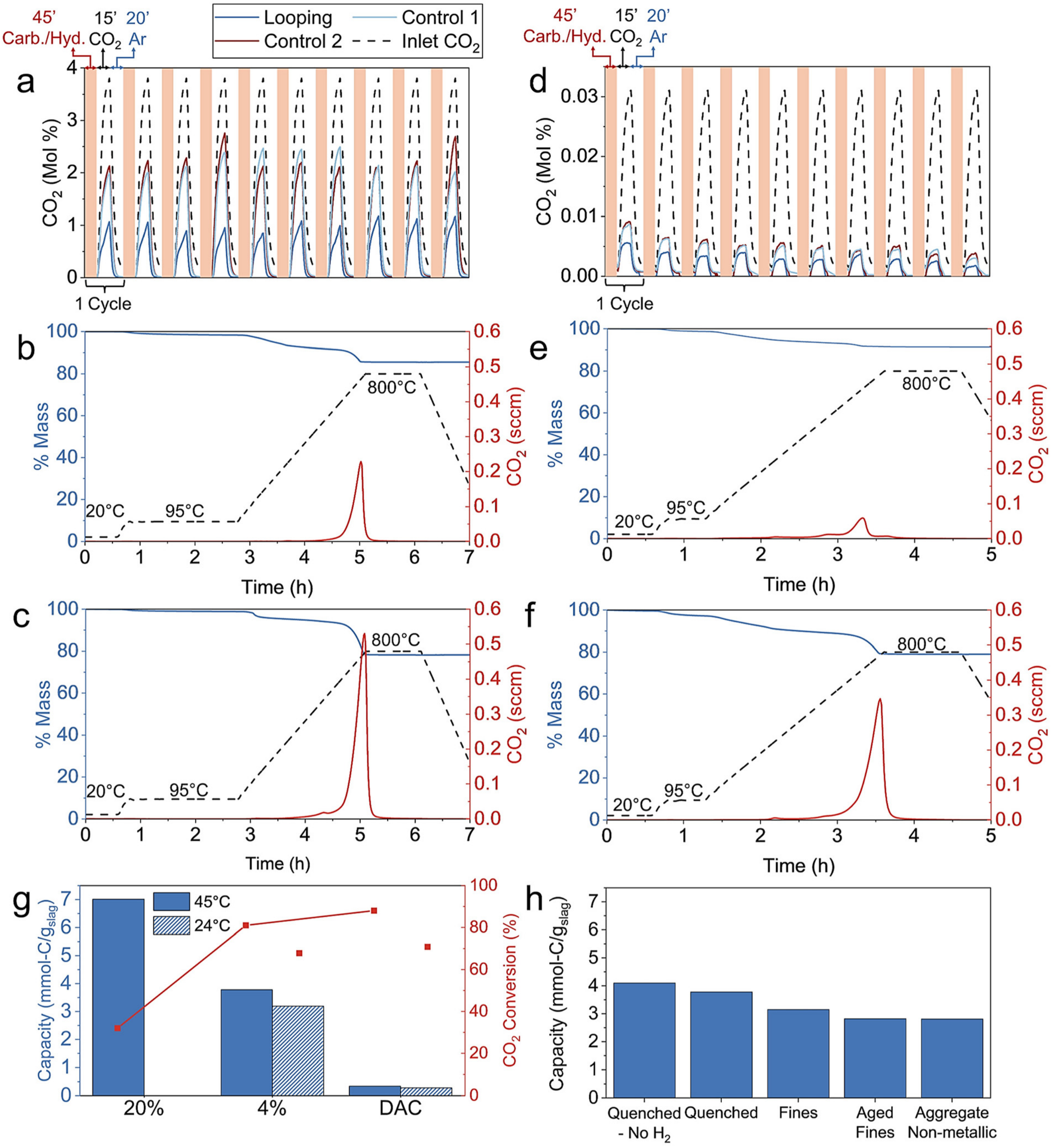

Fig. 5 (a) Ten Na_2CO_3 looping and control cycles of point-source CO_2 capture with quenched BOF slag. 0.5 g of steel slag per cycle with 90 sccm 4% CO_2/Ar. (b) Thermogravimetric analysis (TGA) and CO_2 evolution of carbonate-rich product after 10 cycles from a control method (Fig. S4b Case 3) with steel slag and water mixture capturing 4% CO_2. (c) TGA and CO_2 evolution of carbonate-rich product after 10 cycles from Na_2CO_3 looping capturing 4% CO_2, showing 1.9 times higher CO_2 mineralization than the control in (b). (d) Ten Na_2CO_3 looping and control cycles of air CO_2 capture with quenched BOF slag. 0.05 g of steel slag per cycle with 90 sccm of 343 ppm CO_2/Air. (e) TGA and CO_2 evolution of carbonate-rich product after 10 cycles from a control method with steel slag and water mixture capturing 343 ppm CO_2. (f) TGA and CO_2 evolution of carbonate-rich product after 10 cycles from air CO_2 Na_2CO_3 looping, showing 4.3 times higher CO_2 mineralization than the control (e). (g) Comparison of CO_2 capture capacity and CO_2 conversion by quenched slag over 5 cycles for 20% CO_2, 4% CO_2, and 343 ppm CO_2 (air) at 45 °C and room temperature (24 °C). (h) CO_2 capture capacity of different BOF slags over 5 cycles for 4% CO_2. Quenched – No H_2 is quenched slag that did not react with steam for H_2 production prior to Na_2CO_3 looping. All cycles were conducted at 45 °C, unless noted otherwise.

79% CO_2 conversion. Fig. S12 illustrates carbon mass balance and the effect of increasing CO_2 reaction time, showing how the amount of Na_2CO_3 and $NaHCO_3$ formed during the CO_2 capture step can be tuned. With 20% CO_2 concentration and 60-minute reaction time, the capture capacity reaches 14.02 mmol-C g^{-1} slag.

Thermogravimetric analysis (TGA) and CO_2 evolution evaluated the amount of CO_2 mineralized in the carbonate-rich product. Fig. 5b shows the TGA and CO_2 evolution from the control (Case 3 in Fig. S4b) experiment. The mass drop and CO_2 evolution around 800 °C are due to the decomposition of $CaCO_3$ within the carbonate-rich product into CO_2 and CaO. In comparison, Fig. 5c shows the mineralized CO_2 from the Na_2CO_3 looping cycles. For comparison to both controls as well as pH and temperature data see Fig. S13.

The looping mineralizes 1.9 times more CO_2 than the controls. This difference arises because the looping mineralizes CO_2 *via* the reaction between Na_2CO_3 and slag, while the control uses CO_2 and slag in water. The 50 times greater solubility of Na_2CO_3 than CO_2 in water contributes to faster kinetics. Furthermore, in the control case, part of the CO_2 is converted to $NaHCO_3$ by the Na_2CO_3 reactor, which does not interact with the slag.

Air CO_2. To capture and mineralize air CO_2, 0.05 g of steel slag was processed in each cycle with 90 sccm of 343 ppm CO_2 (from a compressed air cylinder). The performance of quenched slag over 10 Na_2CO_3 looping cycles is depicted in Fig. 5d, compared to the controls and blank run. Over 10 cycles, the CO_2 capture performance increases due to the capture capacity of the slag from previous cycle(s) not being fully utilized, leading to a CO_2 conversion of 90%. TGA and CO_2 evolution results (Fig. 5e and f) show 4.3 times higher CO_2 mineralization by Na_2CO_3 looping compared to the control (Case 3 in Fig. S4b). For comparison to both controls as well as pH and temperature data see Fig. S14.

Effects of reaction conditions and slag types. The CO_2 capture performance for quenched slag was compared over 5 cycles among 20%, 4%, and 343 ppm CO_2 (from compressed air cylinder) at 45 °C and room temperature (24 °C) (Fig. 5g and Fig. S15–S17).

Under the fixed cycle time, slag mass, and reaction conditions used in these experiments, the inverse trends observed between CO_2 capacity and conversion efficiency arise from the transition between CO_2 supply-limited and reaction kinetics limited scenarios. At low inlet CO_2 concentrations, nearly all the supplied CO_2 is consumed within each cycle, resulting in high conversion efficiency but lower absolute CO_2 uptake due to limited CO_2 availability. As the inlet CO_2 concentration increases, the amount of CO_2 delivered exceeds the amount that can be captured within the fixed reaction time, and the system becomes reaction kinetics limited. Consequently, the total CO_2 captured per cycle increases, while the conversion efficiency decreases.

Additionally, the difference in CO_2 capacity between 45 °C and 24 °C is only about 20% for both air and point-source, highlighting the high kinetics even at room temperature.

The CO_2 capture performance of the four BOF slags were then compared for 4% CO_2 at 45 °C over 5 cycles (Fig. 5h and Fig. S18–S21). "Quenched – No H_2" refers to quenched slag that did not undergo H_2 production before Na_2CO_3 looping.

Unlike in H_2 production, handling and aging of the slag did not significantly affect CO_2 capture, which primarily depends on the calcium silicate and CaO components. Quenched slag captured more CO_2 than others because the main form, Ca_3SiO_5, is more reactive than Ca_2SiO_4 and $CaSiO_3$.[55] We infer Quenched – No H_2 captured more CO_2 due to two factors: first, CaO reacts with steam at high temperature to form calcium hydroxide, which may capture CO_2 between experiments without being measured. Second, when slag reacts with steam, iron oxide gains oxygen, increasing the total slag mass and reducing relative calcium silicate/CaO content.

Material characterization for mechanism verification. XRD was used to compare unreacted quenched slag with slags after 10 control cycles and after 10 Na_2CO_3 looping cycles capturing 4% CO_2 at 45 °C (Fig. 6a). $(Mg_{0.8}Fe_{0.2})O$ was oxidized to $Mg_{0.64}Fe_{2.36}O_4$ by reacting with steam, leaving $Mg_{0.9}Fe_{0.1}O$. Na_2CO_3 looping showed higher conversions of Ca_2SiO_4, Ca_3SiO_5, and CaO to $CaCO_3$ than the control, qualitatively confirming the mineralization capacity found by TGA and CO_2 evolution. Here, we observe that the $Ca_2Fe_2O_5$ phase is largely unreactive. ICP-OES indicates the presence of a small amount of aluminum (Table S1), suggesting that this phase could exist as a calcium aluminoferrite; however, the low aluminum content makes it difficult to distinguish *via* XRD analysis. Fig. S22 shows the results of XRD analysis for the other BOF slags.

Solution-phase Ca and Si concentrations were measured by ICP-OES and UV-vis, respectively (Fig. 6b). Quenched slag was first hydrated in water for 150 min, during which Ca was rapidly released and approached near-saturation within 10 min. This fast initial increase is attributed to the fast reaction of free CaO with water and the formation of $Ca(OH)_2$, which is known to dissolve rapidly in aqueous systems. After this initial period, the concentrations of dissolved Ca remained approximately constant, indicating depletion of the readily soluble Ca phases. Meanwhile, the amount of dissolved Si remains minimal, indicating that calcium silicate has very limited dissolution.

Upon the addition of Na_2CO_3, the dissolved Ca was immediately removed from the solution *via* $CaCO_3$ precipitation, leading to a sharp drop in Ca concentration. This rapid Ca removal was followed by a gradual increase in dissolved Si concentration. Because Ca is continuously taken from solution by carbonate precipitation, thermodynamic equilibrium is driving continuous dissolution of Ca from calcium silicate phases, with Si released as the counter-ion. The key observation is that $CaCO_3$ precipitation occurs almost instantaneously relative to the much slower replenishment of Ca *via* silicate dissolution.

The sharp decay in dissolved Ca combined with the slow rise in Si indicates that carbonate precipitation is not rate limiting under these conditions. Instead, the overall mineralization rate is governed by the kinetics of Ca release from Ca–silicate phases. This interpretation is further supported by the convergence of dissolved Si concentrations toward values analyzed from XRD-refined Ca_2SiO_4 and Ca_3SiO_5 contents ($\sim$228 mg L^{-1} by XRD analysis *versus* 207–276 mg L^{-1} measured), consistent with near-complete conversion of calcium silicates 100 min after Na_2CO_3 was introduced.

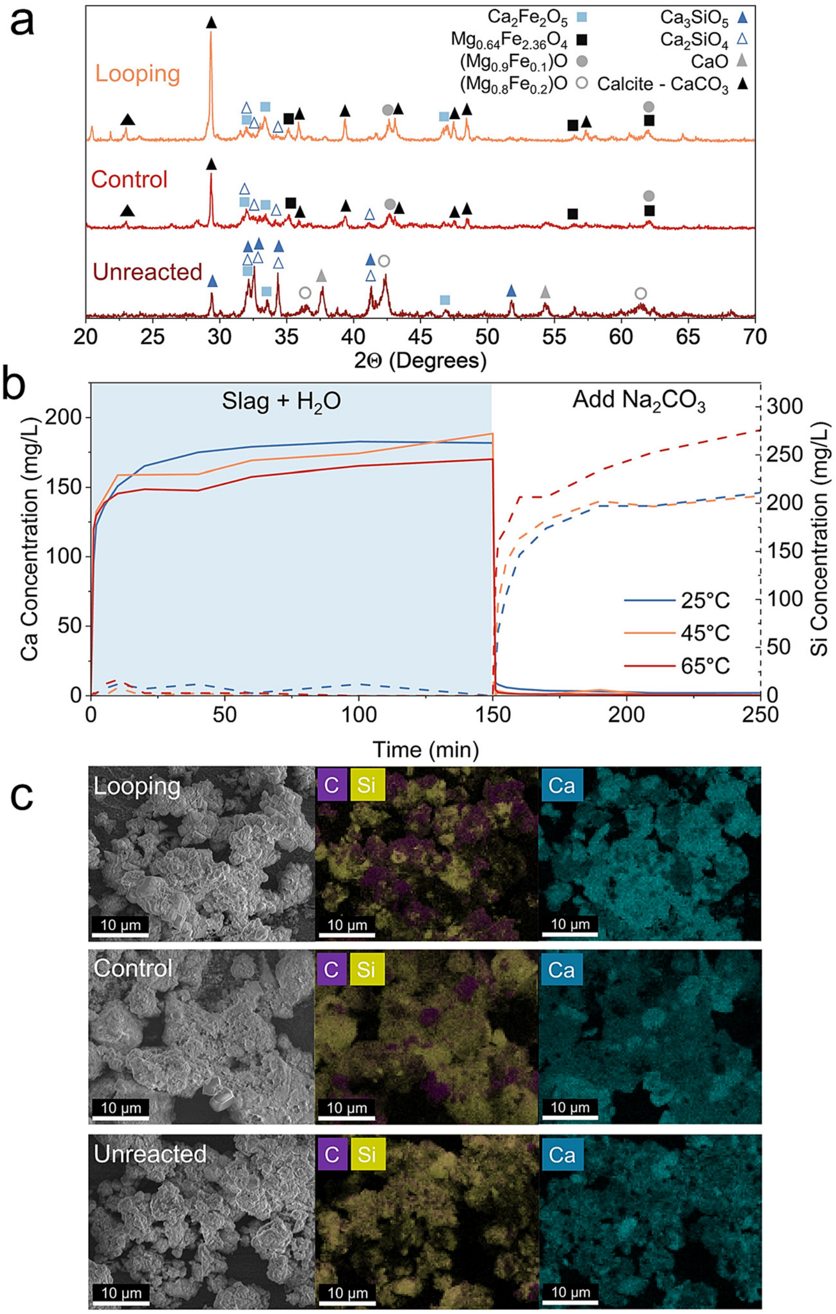

Fig. 6 (a) X-ray diffraction (XRD) comparing unreacted quenched BOF slag with slags after the control process and after the Na_2CO_3 looping process, each process including 10 cycles with 4% CO_2 at 45 °C. (b) Calcium (Ca) and silicon (Si) concentration evolution in aqueous solution during hydration of quenched slag in water, followed by the addition of Na_2CO_3. (c) Scanning electron microscopy (SEM) and energy dispersive X-ray spectroscopy (EDS) maps to compare the distribution of Ca, Si, and carbon (C) in unreacted quenched BOF slag with slags after the control process and after the Na_2CO_3 looping process, with each process including 10 cycles with 4% CO_2 at 45 °C. XRD and elemental mapping show a higher degree of CO_2 mineralization by Na_2CO_3 looping than the control process.

Temperature-dependent measurements further support this assignment of the rate-limiting step. Increasing the solution temperature from 25 to 65 °C has only a minor effect on the rapid Ca dissolution and $CaCO_3$ precipitation steps but significantly accelerates the rate of Si release (Fig. 6b). Because the stirring rate, water-to-slag ratio, and solution chemistry were held constant, this temperature dependence is most consistent with chemical reaction controlled Ca–silicate dissolution rather than diffusion-limited precipitation processes.[56] Taken together, these results indicate that Na_2CO_3 looping accelerates mineralization primarily by rapidly removing Ca *via* carbonate precipitation, thereby sustaining a strong thermodynamic driving force for continued Ca–silicate dissolution, which ultimately governs the overall carbonation rate.

SEM and EDS maps were used to show carbonation products from quenched slag (Fig. 6c). Carbon (C) and Si maps reveal greater CO_2 mineralization by Na_2CO_3 looping than the control. The replacement of Si by C is also apparent in the SEM images where rhombohedral $CaCO_3$ (calcite) crystals are growing.

Conclusions

This study introduces a novel Na_2CO_3 looping process that integrates CO_2 capture and mineralization using steel slags, producing a carbonate-rich product and high-value amorphous silica as supplementary cementitious materials. This process was demonstrated on BOF steel slags and achieved high capture rates of 59% and 35% for 4% and 343 ppm CO_2, respectively. Compared to a slag and water mixture baseline case, the looping scenarios mineralized 4–9 times more CO_2. Mechanistic analysis indicates that the enhanced mineralization rates from Na_2CO_3 arise from rapid Ca removal *via* carbonate precipitation, which maintains a strong thermodynamic driving force for continued Ca–silicate dissolution and ultimately controls the overall carbonation kinetics. Additionally, reacting the slag with steam can produce up to 1.01 mmol-H_2 per g-slag. Overall, the looping process is exothermic, and there is no chemical consumed. Technoeconomic analysis shows Na_2CO_3 looping costs of \$252 and \$50 per ton-CO_2 (not including revenues) from air and point-source resulting in only 15–30% of the cost of the baseline. If including revenues, the payback periods are only 1.9 and 0.8 years for air and point-source CO_2.

Methods

Steel slag preparation

The BOF steel slag samples were collected from Cleveland-Cliffs – Cleveland Works. Four different types of slag were obtained: quenched, aggregate non-metallic, fines, and aged fines. The quenched slag was scooped directly from the BOF before slagging off. The aggregate non-metallic slag is typically reused in the blast furnace. The slag fines consisted of unrecyclable slag waste generated in the BOF, while the aged fines were similar but had been exposed to outdoor conditions for an unspecified period. The Cleveland-Cliffs – Cleveland Works BOF steel slag processing flow chart, with endpoints for the four types of slag analyzed, is shown in Fig. S1.

To prepare the slag for testing, large chunks were first crushed to approximately 0.5 cm using a sledgehammer. Then, 70 g of slag was loaded into a 75 mL alumina jar with a stainless-steel jacket under an argon atmosphere to prevent unwanted reactions with air during milling. The slag was milled for 30 minutes in an across international desktop high energy vibratory ball mill, rested for 20 minutes, and milled for another 30 minutes. The resulting powder was scraped out using a metal spatula and sifted through a 60-mesh (250-micron) sieve. Material that did not pass through was first processed with a 2 mm sieve, and any remaining oversized particles were reloaded into the alumina jar for additional milling, with fresh slag supplemented to reach 70 g. The final steel slag powder was stored in a glovebox under argon before experiments.

Hydrogen production performance testing

Hydrogen (H_2) production experiments were conducted in a custom quartz tube with an outer diameter of 25 mm, a length of 609.6 mm, and a 3 mm thick G0 (160–250 micron) quartz frit positioned 15 mm off-center. A 6 g sample of steel slag was packed between layers of quartz wool, which rested on the frit at the center of the tube. The tube was then loaded into a vertically oriented 1100 °C split-tube furnace (Thermcraft Protégé XST). A gas mixture of 100 sccm containing 2% water vapor diluted in argon (created by a Cellkraft P-2 Humidifier) flowed through the packed sample bed. The furnace was heated to a certain temperature within 500 to 1000 °C at a ramp rate of 10 °C min^{-1} and held at this temperature for 8 hours for the steam to H_2 conversion.

H_2 production was monitored using a gas chromatograph (Inficon Micro GC Fusion), with indicating Drierite used to remove any unreacted water vapor before analysis to protect the GC. To ensure consistent data collection, the gas chromatograph was started when the furnace setpoint reached 100 °C. After the experiment, the processed steel slag was returned to the argon glove box for storage.

Na_2CO_3 looping performance testing

Point-source CO_2. In the 4% CO_2 looping case, 1 g of post-hydrogen-production quenched slag was reacted in an aqueous solution containing 2.5 g Na_2CO_3 (Sigma-Aldrich) and 50 mL deionized (DI) water in a 50 mL centrifuge tube. The reaction was carried out at 45 °C and 400 rpm for 30 min by suspending the centrifuge tube in a 500 mL beaker filled with 450 mL water, maintained on a hotplate set to 108 °C.

After carbonation, the mixture was centrifuged at 1200 rpm for 10 min to separate the carbonate-rich product from the solution. The solution was then divided equally between two 100 mL gas washing bottles to enhance gas–liquid contact time. The bottles were insulated with 0.5-inch ceramic fiber insulation and heated on hotplates to maintain a reaction temperature of 45 °C (corresponding to a hotplate setpoint of 60 °C).

Prior to CO_2 exposure, the bottles were purged with argon (90 sccm) for 5 min. The CO_2 concentration during this flush averaged below 0.01%, and its cumulative amount was negligible compared to the captured CO_2 measured afterward. For the CO_2 capture step, a 4% CO_2/Ar gas mixture was flowed at 90 sccm for 30 min, followed by a 15 min argon purge. This purge gradually decreased CO_2 concentration due to the empty space in the wash bottles. The outlet gas composition was quantified using the GC equipped with indicating Drierite to remove residual water vapor. The GC was started 1 min before CO_2 introduction to ensure synchronized data collection.

After each capture step, 1 g of post-hydrogen-production quenched slag was added to the regenerated solution, and the cycle was repeated for a total of four times. Additionally, after each carbonation and CO_2 capture step, pH and temperature were measured using an Ohaus Starter 2200 pH Bench Meter (ST322 electrode) and a K-type thermocouple, respectively.

A corresponding baseline experiment was conducted under identical conditions but without Na_2CO_3 addition. Fig. S4a visualizes the looping and baseline cases.

In the 20% CO_2 looping case, 10 g of aged fines were reacted in an aqueous solution containing 25 g Na_2CO_3 and 200 mL DI water in a 250 mL gas washing bottle. The reaction was carried out at 45 °C and 400 rpm for 30 min, maintained on a hotplate set to 74 °C with 0.5-inch ceramic fiber insulation around the bottle.

After carbonation, the mixture was vacuum filtered to separate the carbonate-rich product from the solution. The solution was then divided equally between two 250 mL gas washing bottles to enhance gas–liquid contact time. The bottles were insulated with 0.5-inch ceramic fiber insulation and heated on hotplates to maintain a reaction temperature of 45 °C (corresponding to a hotplate setpoint of 70 °C).

Prior to CO_2 exposure, the bottles were purged with argon (90 sccm) for 5 min. For the CO_2 capture step, a 20% CO_2/Ar gas mixture was flowed at 90 sccm for 20 min, followed by a 15 min argon purge. The outlet gas composition was quantified using the GC equipped with indicating Drierite to remove residual water vapor. The GC was started 1 min before CO_2 introduction to ensure synchronized data collection.

After each capture step, 10 g of aged fines were added to the regenerated solution, and the cycle was repeated for a total of four times. Additionally, after each carbonation and CO_2 capture step, pH and temperature were measured.

A corresponding baseline experiment was conducted under identical conditions but without Na_2CO_3 addition.

Air CO_2. For air, the same Na_2CO_3 looping procedure was applied with modified reaction conditions. In the looping case, 0.05 g of post-hydrogen-production quenched slag was reacted in an aqueous solution containing 0.05 g Na_2CO_3 and 5 mL deionized (DI) water in a 50 mL centrifuge tube. The reaction was carried out at room temperature (24 °C) and 400 rpm stirring rate for 15 min.

After carbonation, the mixture was centrifuged at 1200 rpm for 10 min to separate the carbonate-rich product from the solution. Due to the small volume, the solution was then divided equally between two 50 mL centrifuge tubes. Each centrifuge tube was installed into a 100 mL gas washing bottle to get connected with gas delivery and exhaust lines.

Before CO_2 exposure, the bottles were purged with argon (90 sccm) for 5 min. The CO_2 concentration during this flush averaged below 0.002%, and its cumulative amount was negligible relative to the captured CO_2 measured afterward. For the CO_2 capture step, air containing 343 ppm CO_2 (from a compressed air cylinder) was flowed at 90 sccm for 1.5 h, followed by a 15 min argon purge to displace the remaining gas for CO_2 quantification purposes. The outlet gas composition was quantified using the GC equipped with indicating Drierite to remove residual water vapor. The GC was started 1 min before CO_2 introduction to ensure synchronized data collection.

After each capture step, 0.05 g of post-hydrogen-production quenched slag was added to the regenerated solution, and the cycle was repeated for a total of four times. To compensate for minor evaporative losses (<0.25 mL), DI water was added as needed to maintain a constant 5 mL solution volume between cycles. After carbonation and CO_2 capture, pH and temperature were measured using an Ohaus Starter 2200 pH Bench Meter (ST322 electrode) and a K-type thermocouple, respectively.

A corresponding baseline experiment was performed under identical conditions but without Na_2CO_3 addition.

Na_2CO_3 looping mechanism testing

CO_2 capture and mineralization experiments were conducted using a series of two 250 mL gas washing bottles, each placed on a separate hotplate with a stir bar and wrapped in insulation. Unless otherwise noted, experiments were performed on steam reacted steel slag for both point-source and air.

Point-source CO_2. Four experimental cases were tested: Na_2CO_3 looping, two controls, and a blank run (see Cases 1 through 4 in Fig. S4b). Each gas washing bottle was filled with 60 mL of deionized (DI) water. For Na_2CO_3 looping experiments (Case 1 in Fig. S4b), 0.625 g of Na_2CO_3 and 0.25 g of steel slag were added to each bottle. The bottle caps were secured, and dip tubes were placed halfway into the solution. Gas lines were connected using a two-way valve at the inlet of the first bottle and the outlet of the second. The system was flushed with argon before sealing. The bottles were insulated with 0.5-inch ceramic fiber insulation and heated on hot plates to the reaction temperature (24 °C or 45 °C) at 80 rpm for 45 minutes – this step is referred to as the carbonation reaction. To reach a mixture temperature of 45 °C measured by a thermocouple, the hotplates needed to be set to 60 °C.

After carbonation, pH and temperature were recorded using an Ohaus Starter 2200 pH Bench Meter (ST322 electrode) and a K-type thermocouple. The bottles were then flushed with 90 sccm argon for 5 minutes before initiating the CO_2 capture step. The CO_2 concentration was monitored during the flush to be on average less than 0.01%, whose cumulative amount is negligible compared to the CO_2 captured afterwards. The CO_2 capture step is where 90 sccm of either 4% or 20% CO_2/Ar was bubbled through the solution for 15 minutes, followed by 20 minutes of pure argon flow that gradually decreases CO_2 concentration due to the empty space in the wash bottle. CO_2 concentration in the outlet gas was quantified using the gas chromatograph, with indicating Drierite used to remove any residual water vapor. To ensure consistent data collection timing, the gas chromatograph was started 1 minute before the CO_2 flow began.

One cycle consisted of both the carbonation and CO_2 capture steps. After each cycle, 0.25 g of steel slag was added to each bottle, and the process was repeated for 5 or 10 cycles.

The control experiments followed the same procedure but with different initial reactant distributions so that the slag–water mixture did not interact with Na_2CO_3. Case 2 had 1.25 g of Na_2CO_3 in the first bottle and 0.5 g of steel slag in the second. Case 3 had 0.5 g of steel slag in the first bottle and 1.25 g of Na_2CO_3 in the second. Each wash bottle in the control cases also included 60 mL DI water.

CO_2 capture efficiency in looping and control experiments was calculated relative to a blank run, where CO_2 was bubbled through only water to characterize the supply gas CO_2 profile (Case 4).

Air CO_2. These experiments followed the same procedure, with each gas washing bottle containing 30 mL of DI water. Case 1 used 0.0625 g of Na_2CO_3 and 0.025 g of steel slag per bottle, while the control (Case 2 and 3) contained 0.125 g of Na_2CO_3 in one bottle and 0.05 g of steel slag in the other. The blank run (Case 4) contained only DI water. 90 sccm of air (from a compressed cylinder containing 343 ppm CO_2) was flowed for 15 minutes, followed by 20 minutes of argon flow. For the 5-minute flush after carbonation, the CO_2 concentration was monitored to be on average less than 0.002%, whose cumulative amount is negligible compared to captured CO_2.

Material characterization using XANES

X-ray absorption near edge structure (XANES) was conducted by easyXAFS300+ to measure the oxidation state of iron (Fe) in steel slag before and after the reaction with steam. The X-ray source was set at 36 kV and 20 mA to acquire energy absorption spectra ranging from 7000 eV to 7600 eV for Fe K edge. Steel slag and standard materials (FeO, Fe_3O_4, and $CoFe_2O_4$) were protected against air oxidation using Kapton tape. XANES data was analyzed by *Athena* software to give normalized absorption (μ) *vs.* absorption energy.

Material characterization using TGA

Experiments were conducted using a Themys thermogravimetric analyzer (TGA). For quantifying the CO_2 release from the carbonate-rich product and from $Na_2CO_3/NaHCO_3$ solution, 0.1 g of solid or 1 mL of solution was placed in a 1300 mm^3 alumina crucible. Argon (50 sccm) flowed over the sample, and the product gas was analyzed using a gas chromatograph, with indicating Drierite used to remove any residual water vapor. For 4% CO_2 capture slag and solution, the temperature profile consisted of 35 minutes at 20 °C, 120 minutes at 95 °C, and 60 minutes at 800 °C. For air CO_2 slag, the same temperature profile was used, except the dwell time at 95 °C was reduced to 30 minutes. The ramp heating and cooling rates were 5 °C min^{-1} and 10 °C min^{-1}, respectively.

Material characterization using XRD

X-ray diffraction (XRD) was performed using a Rigaku SmartLab X-ray diffractometer with Cu Kα radiation (λ = 1.5406 Å) at 40 kV and 44 mA under ambient pressure and temperature. The Bragg–Brentano focusing method was used, and a diffracted beam monochromator was employed to reduce iron fluorescence. Steel slag data were collected over a 2θ range of 20° to 70° with a step size of 0.02° and a scan speed of 2.3° min^{-1}. SiO_2 data was collected using the same procedure with a 2θ range of 10° to 70°. The samples were finely ground in a mortar and pestle and mounted on a glass holder. Phase identification and refinement were performed using *PDXL* software with the *PDF2 2023* database.

Material characterization using UV-vis and ICP-OES

Ca and Si concentrations were measured by inductively coupled plasma optical emission spectrometry (ICP-OES) and Ultraviolet-visible spectroscopy (UV-vis), respectively. Ca concentrations were determined using a PerkinElmer Optima 3000DV ICP-OES system, while Si concentrations were measured using a SpectraMax Plus 384 spectrophotometer with the silicon-molybdenum yellow spectrophotometric method.

For sample preparation, 120 mL of DI H_2O was added to a 250 mL gas washing bottle, which was then placed on a hotplate to maintain a constant solution temperature of 25 °C, 45 °C, or 65 °C with stirring at 80 rpm. The hotplate setpoints were 30 °C, 65 °C, and 100 °C, respectively. After reaching the set temperature, 0.5 g of slag was added to the water, and samples were collected at regular time intervals of 1, 2, 5, 10, 20, 40, 60, 100, and 150 minutes. After 150 minutes, 1.25 g of Na_2CO_3 was introduced, and sampling continued at similar intervals. 100 sccm argon was continuously flown through the gas washing bottle to prevent unwanted reactions with air.

Amorphous SiO_2 purity was assessed using the PerkinElmer Optima 3000DV ICP-OES system. Sample preparation was done with 19 g of quenched BOF slag carbonated in an aqueous solution containing 47 g of Na_2CO_3 in 900 mL DI H_2O for 12 hours at 60 °C and 80 rpm. The mixture was then filtered, and the solution was subject to 48 hours of 90 sccm pure CO_2 to precipitate silicic acid which was filtered and dried to produce SiO_2. To remove impurities, the SiO_2 was washed with DI H_2O and ultrasonicated for 30 minutes. Finally, the washed SiO_2 was dissolved in 0.1 M NaOH for ICP-OES analysis.

Material characterization using SEM/EDS

Scanning electron microscopy (SEM) was performed using a thermo Fisher scientific Apreo scanning electron microscope. Imaging was conducted in secondary electron (SE) mode with an Everhart–Thornley detector (ETD) at 5 kV and 0.8 nA. Energy-dispersive X-ray spectroscopy (EDS) was performed using the same microscope at 10 kV and 6.4 nA, equipped with an EDAX Octane Elect 30 mm^2 silicon drift detector (SDD).

The samples were dispersed in DI water and sonicated at 25 °C for 5 minutes. 10 μL of the dispersion was pipetted onto an SEM stub and dried on a hotplate at 80 °C for 5 hours. Steel slag samples were directly dropped on aluminum SEM stubs, while a layer of carbon tape was used for precipitated SiO_2 samples.

Measurement uncertainty

Measurement uncertainties were quantified for pH and temperature monitoring, TGA, GC, ICP-OES, and UV-vis. Instrument specifications give uncertainties of ±0.01 pH units and ±2.2 °C for solution measurements.

Uncertainty in TGA-based carbon quantification was evaluated using duplicate blank runs with a dwell at 800 °C. Signal noise was determined from the standard deviation over a 10-min dwell period, and long-term drift was obtained from linear regression of the mass signal over the full dwell. These contributions were propagated through the mass-loss calculation to obtain the uncertainty in mmol-C g^{-1} slag, resulting in a relative uncertainty of $<0.03\%$.

GC uncertainties for 4% CO_2, 20% CO_2, and H_2 were determined from multi-point calibration curves using the standard error of the linear regression, reported as relative uncertainty. For ppm-level CO_2, the certified cylinder specification (±2% relative) was applied. These uncertainties were propagated through integrated gas volumes to yield representative relative uncertainties in the calculated capacities (mmol-C g^{-1} slag) of 3% (4% CO_2), 1.5% (20% CO_2), 7% (air CO_2), and 0.6% (H_2).

Uncertainties were also estimated for ICP-OES and UV-vis measurements. ICP-OES measurements were performed in quadruplicate. Relative standard deviations were typically 1–2%, corresponding to 95% confidence intervals of approximately ±1.6–3.2% on the reported concentrations. UV-vis calibration uncertainty was estimated from the standard error of regression and converted to concentration, yielding ±9.6 mg L^{-1}.

Author contributions

S.Z. and K.S. conceived the project. K.S. conducted experimental work, data analysis, energy and technoeconomic analysis, and manuscript preparation. H.X. and Y.X. contributed to experimental H_2 production and CO_2 capture performance testing. A.K. contributed to XANES experiments and analysis, and energy and technoeconomic analysis. J.Q. contributed to ICP-OES and UV-vis experiments and analysis. S.Z. supervised this study and revised the manuscript.

Conflicts of interest

The authors declare a non-provisional patent application has been filed by The Ohio State University covering aspects of the technology described in this manuscript.

Data availability

The datasets used in this work are available from the corresponding author upon reasonable request.

Supplementary figures and tables, hydrogen production results, and details of technoeconomic analysis are included in supplementary information. See DOI: https://doi.org/10.1039/d5ee07347b.

Acknowledgements

The authors thank Cleveland-Cliffs – Cleveland Works for providing steel slag samples and for their valuable insights into steel production and slag handling in industry. They also acknowledge valuable discussions with Dr Liang-Shih Fan and Dr David Cole on process optimization and mineral chemistry, Dr Hongyan Ma, Dr Lisa Burris, and Dr Jiaqi Li on cement chemistry, and Dr Daniel Gingerich on energy and technoeconomic analysis. Support from the Center for Electron Microscopy and Analysis (CEMAS), the Surface Analysis Laboratory, and the Trace Element Research Laboratory at The Ohio State University is also acknowledged. We also thank Dr Gunjan Agarwal for providing access to UV-vis equipment. The research is partially supported by the Sustainability Research Seed Grant at Sustainability Institute at The Ohio State University. K. Shank is supported by the Distinguished University Fellowship and ENGIE-Axium Fellowship at The Ohio State University. A. Arjomand is partially supported by the U.S. Department of Energy under award DE-EE0010733.

References

1 S. Chu and A. Majumdar, *Nature*, 2012, **488**, 294–303.
2 L. B. Hamdy, C. Goel, J. A. Rudd, A. R. Barron and E. Andreoli, *Mater. Adv.*, 2021, **2**, 5843–5880.
3 D. W. Keith, G. Holmes, D. Angelo and K. Heidel, *Joule*, 2018, **2**, 1573–1594.
4 B. V. L'vov, *Thermochim. Acta*, 1997, **303**, 161–170.
5 L. Monasterio-Guillot, F. Di Lorenzo, E. Ruiz-Agudo and C. Rodriguez-Navarro, *Chem. Geol.*, 2019, **524**, 158–173.
6 A.-H. A. Park and L.-S. Fan, *Chem. Eng. Sci.*, 2004, **59**, 5241–5247.
7 N. Zhang, R. Yang, H. D. Huang, J. Meng, W. Zhang, A.-H. A. Park and A. Moment, *ACS ES&T Eng.*, 2025, **5**, 103–114.
8 L. A. Bullock, A. Yang and R. C. Darton, *Sci. Total Environ*, 2022, **808**, 152111.
9 C. Wang, H. Jiang, E. Miao, Y. Wang, T. Zhang, Y. Xiao, Z. Liu, J. Ma, Z. Xiong, Y. Zhao and J. Zhang, *Chem. Eng. J.*, 2024, **488**, 150676.
10 L. Li, Q. Liu, T. Huang and W. Peng, *Sep. Purif. Technol.*, 2022, **298**, 121512.
11 M. Bui, C. S. Adjiman, A. Bardow, E. J. Anthony, A. Boston, S. Brown, P. S. Fennell, S. Fuss, A. Galindo, L. A. Hackett, J. P. Hallett, H. J. Herzog, G. Jackson, J. Kemper, S. Krevor, G. C. Maitland, M. Matuszewski, I. S. Metcalfe, C. Petit, G. Puxty, J. Reimer, D. M. Reiner, E. S. Rubin, S. A. Scott, N. Shah, B. Smit, J. P. M. Trusler, P. Webley, J. Wilcox and N. Mac Dowell, *Energy Environ. Sci.*, 2018, **11**, 1062–1176.
12 G. Biava, L. E. Depero and E. Bontempi, *Span. J. Soil Sci.*, 2024, **14**, 12908.
13 S. Yoon, W. Choi and C. Jeon, *Sci. Rep.*, 2024, **14**, 2399.
14 Total production of crude steel, https://worldsteel.org/data/annual-production-steel-data/?ind=P1_crude_steel_total_pub/CHN/IND, (accessed 17 April 2025).
15 World Steel Association, 2021.
16 Y. Zhang, L. Yu, K. Cui, H. Wang and T. Fu, *Chem. Eng. J.*, 2023, **455**, 140552.
17 C. Ma, S. Zhang, K. Li, T. Zhao, Q. Meng, D. Guan and A. Zhang, *Metals*, 2025, **15**, 537.

18 S. Srivastava, M. Cerutti, H. Nguyen, V. Carvelli, P. Kinnunen and M. Illikainen, *Cem. Concr. Compos.*, 2023, **142**, 105213.

19 Y. Chen and M. W. Kanan, *Nature*, 2025, **638**, 972–979.

20 P. Kelemen, S. M. Benson, H. Pilorgé, P. Psarras and J. Wilcox, *Front. Clim.*, 2019, **1**, 9.

21 I. Walker, R. Bell and K. Rippy, *npj Mater. Sustainability*, 2024, **2**, 28.

22 C. A. Myers, T. Nakagaki and K. Akutsu, *Int. J. Greenhouse Gas Control*, 2019, **87**, 100–111.

23 S.-Y. Pan, T.-C. Chung, C.-C. Ho, C.-J. Hou, Y.-H. Chen and P.-C. Chiang, *Sci. Rep.*, 2017, **7**, 17227.

24 H. Zhai, Q. Chen, M. Yilmaz and B. Wang, *Environ. Sci. Technol.*, 2023, **57**, 13808–13817.

25 M. Liu, A. Hohenshil and G. Gadikota, *Energy Fuels*, 2021, **35**, 8051–8068.

26 L. Li, H. Yu, G. Puxty, S. Zhou, W. Conway and P. Feron, *Ind. Eng. Chem. Res.*, 2024, **63**, 16019–16028.

27 L. Li, H. Yu, L. Ji, S. Zhou, V. Dao, P. Feron and E. Benhelal, *J. Environ. Chem. Eng.*, 2024, **12**, 113382.

28 L. Wu, H. Li, H. Mei, L. Rao, Y. Xia and Y. Dong, *Miner. Eng.*, 2023, **204**, 108374.

29 B. Z. Dlugogorski and R. D. Balucan, *Renewable Sustainable Energy Rev.*, 2014, **31**, 353–367.

30 P. Li, Y. Chen, X. Li, B. Yan, D. Chen and H. Guo, *Int. J. Hydrogen Energy*, 2020, **45**, 17140–17152.

31 J. Li, D. Bhattacharjee, X. Hu, D. Zhang, S. Sridhar and Z. Li, *Miner. Process. Extr. Metall.*, 2017, **126**, 94–105.

32 M. Sato, H. Matsuura and F. Tsukihashi, *ISIJ Int.*, 2012, **52**, 1500–1502.

33 Y. Jiang, T.-C. Ling, C. Shi and S.-Y. Pan, *Resour., Conserv. Recycl.*, 2018, **136**, 187–197.

34 Carbon Negative Shot, Department of Energy, https://www.energy.gov/topics/carbon-negative-shot, (accessed 2 March 2025).

35 P. Li, H. Guo, J. Gao, J. Min, B. Yan, D. Chen and S. Seetharaman, *J. Cleaner Prod.*, 2020, **254**, 119952.

36 S. Hughes, S. Leptinsky, M. Woods, A. Zoelle, N. Kuehn, T. Fout and G. Hackett, Methodology for Estimating Performance and Cost of Natural Gas Combined Cycle Plants with Carbon Capture, 2023.

37 U.S. Environmental Protection Agency (EPA), 2024.

38 G. P. Towler and R. K. Sinnott, *Chemical engineering design: principles, practice, and economics of plant and process design*, Butterworth-Heinemann, Boston, MA, 2nd edn, 2013.

39 D. R. Woods, *Rules of thumb in engineering practice*, John Wiley [distributor], Chichester, 2007.

40 G. Holmes and D. W. Keith, *Philos. Trans. R. Soc., A*, 2012, **370**, 4380–4403.

41 Hydrogen Production, https://www.energy.gov/eere/fuelcells/hydrogen-production, (accessed 4 March 2025).

42 Intratec, Silicon Dioxide Prices, Historical and Current, https://www.intratec.us/chemical-markets/silicon-dioxide-price, (accessed 4 March 2025).

43 45Q Tax Credit for Carbon Capture Projects, https://carboncapturecoalition.org/resource/45q-tax-credit-for-carbon-capture-projects/, (accessed 12 November 2025).

44 H. S. A. Microsilica, What is silica fume price per ton? https://microsilica-fume.com/silica-fume-price-per-ton.html, (accessed 18 January 2026).

45 Q. Song, M.-Z. Guo, M. Zhang and T.-C. Ling, *J. Cleaner Prod.*, 2024, **469**, 143214.

46 Mineral commodity summaries 2025, 2025.

47 T. Fox and C. Randall, 1996.

48 Burns Harbor, https://www.clevelandcliffs.com/operations/steelmaking/burns-harbor, (accessed 18 January 2026).

49 OECD, *OECD Steel Outlook 2025*, OECD Publishing, Paris, 2025, DOI: 10.1787/28b61a5e-en.

50 B. A. Fleming and D. A. Crerar, *Geothermics*, 1982, **11**, 15–29.

51 S. J. Gerdemann, W. K. O'Connor, D. C. Dahlin, L. R. Penner and H. Rush, *Environ. Sci. Technol.*, 2007, **41**, 2587–2593.

52 A. Frýbort, J. Štulířová, J. Grošek and M. Gregerová, *Case Stud. Constr. Mater.*, 2023, **18**, e01916.

53 S. Muljani, H. Setyawan and R. E. Nugraha, *RSC Adv.*, 2023, **13**, 33471–33483.

54 M. Á. Sanjuán, C. Argiz, J. C. Gálvez and A. Moragues, *Constr. Build. Mater.*, 2015, **96**, 55–64.

55 G. Moir, in *Advanced Concrete Technology*, Elsevier, 2003, pp. 3–45.

56 M. Antunes, R. L. Santos, J. Pereira, R. B. Horta, P. Paradiso and R. Colaço, *Materials*, 2021, **14**, 5347.